Enhanced Effective Thickness (EET) of curved laminated glass.

Laura Galuppi
Gianni Royer-Carfagni

Department of Industrial Engineering, University of Parma

Parco Area delle Scienze 181/A, I 43100 Parma, Italy
tel: +39-0521-906606, fax: +39-0521-905705, email: gianni.royer@unipr.it

Abstract Approximate methods for calculating Laminated Glass (LG), a composite where thin polymeric layers are sandwiched by glass plies, are very useful in the design practice. The most common approach relies upon the definition of the effective thickness, i.e., the thickness of a glass monolith that, under the same boundary and load conditions, presents the same maximal stress or deflection of the laminate. Different alternative formulations have been proposed, but for flat glass only. Meeting the increasing interest for curved glazing in modern architecture, here the recent "Enhanced Effective Thickness" method is extended to the case of single-curvature LG panels. Under the assumption that the curvature is moderate, usually met in the practice, simple formulae for the effective thickness are proposed. A practical method is presented to calculate the relevant coefficients, which depend upon the geometry, load and boundary conditions. Comparison with numerical experiments in paradigmatic examples confirms the accuracy of the proposed approach.

Keywords: Laminated glass, curved glass, effective thickness, sandwich beam, curved composite beam, shear-compliant core.

Contents

1 Introduction

Curved glazed surfaces are increasingly attracting the interest of architects because of their powerful aesthetic qualities, consisting in the capacity of diffusing light and delimiting space without the barriers of a flat wall. Curved panels can be obtained through "*hot-bending*", by heating glass above its transition temperature and curving it in the desired shape. In *sag bending*, it is the action of gravity that produces the uniform contact with a negative mould. In *press bending*, glass is formed by a stainless steel mold face and head that presses the panel into the shape of the mold. Both single- and double-curvature surfaces can be obtained, but a limitation is represented by the need of a negative form.

Avoiding the negative mold represents a crucial economical issue, especially for free-form glazed surfaces where the curvature of each panel may differ from the others. To this respect, single-curvature glass panels are acquiring great importance. In fact, on the one hand recent algorithms in analytical geometry allow to discretize double-curvature surfaces of any form with single-curvature panels, even if at the price of reasonable modifications of the initial double curved 3D-shape in order to be able to panelise [32, 11]. On the other hand, numerically-controlled machines are available, which allow to manipulate glass above the transition temperature and calender it, to form single-curvature surfaces whose radius can be arbitrarily and continuously varied, with no need of any negative form. Another technique is "*cold-bending*", which consists in forcing glass in the desired position by its elastic straining within the allowable stress limit, but only developable cylindrical surfaces can be obtained without incurring in strong membrane stress.

In almost all applications, it is preferable to use Laminated Glass (LG). This is a composite formed by glass plies sandwiching polymeric interlayers, made adherent with a process at high temperature and pressure in autoclave. The glass so acquires safety properties because, after breakage, shards remain attached to the polymer and the system maintains a small but significant load bearing capacity, avoiding major damage to properties and human life. In the pre-glass-breakage phase, the stiffness and strength of LG is strongly affected by the degree of connection offered by the polymeric interlayers, which provide shear stresses that constrain the relative sliding of the glass plies [6, 25]. The flexural performance is always intermediate between the borderline cases [29, 12] of *layered limit*, with frictionless sliding glass plies, and *monolithic limit*, with shear-stiff interlayer. To avoid redundant design, the degree of shear coupling through the interlayer must be accurately evaluated. This is why a large number of studies, also in recent years, consider this problem [5, 26, 13].

Since polymers are viscoelastic, their stiffness depends upon load duration and temperature, but taking into account such rheological effects is not immediate. A rationale that is conservative for monotone loading history [18, 20] is the "quasi-static" approximation, which considers the polymer as an elastic material, with its secant stiffness defined according to environmental temperature and characteristic duration of applied actions [7]. Within this simplification, the most practical approach for calculating LG consists in defining its *effective thickness*, that is the thickness of a monolith with equivalent bending properties in terms of stress and deflection. Various formulations have been proposed, among which one should recall the one implemented by ASTM E1300 [30] according to the proposal by Bennison *et al.* [10, 7], based upon the seminal work by Wölfel [37]. More recently, the authors have presented the Enhanced Effective Thickness (EET) method [17], which can be applied to beams, plates [19, 15, 16] and multilaminates [24], and has been mentioned in the Italian code for structural glass [27]. However, all the aforementioned methods have been conceived of for flat glass. To our knowledge, their extension to the case of curved LG still represents an open problem.

Several studies on curved sandwich beams have been done since the Nineties [2, 3, 8]. An analytical model has been presented by Frostig [14] for beams composed by two thin external layers bonded by a thick and soft core, but the case of LG is somehow dual, because the external plies are thick and stiff and the core is thin and shear-compliant. Recently Asik has considered specifically curved LG [4], but under strong simplifying hypotheses and only for beams with constant curvature under purely radial loading, mainly focusing on the numerical implementation of the problem. The authors have recently proposed a more general model for curved laminated glass [22], with a detailed description of the class of admissible deformations and with no restriction about the type of curvature and loading. The method of solution presented in [23] generalizes to the case of curved beams the original method proposed by Newmark *et al.* [28] for straight composite beams, but it requires the *a priori* knowledge of the bending moment and the axial force in the beam. No explicit formulas for the effective thickness have been proposed so far for curved LG, even if a standard, but "unofficial", practice consists in considering single-curvature panels like flat panels, thus neglecting the effect of the curvature. But the reliability of such a procedure, as well as its limit of application, has not been confirmed.

The purpose of this article is to extend the EET method to the case of curved LG. The case of reference is a rectangular panel that has been hot formed into a single-curvature cylindrical surface, so that it can be considered as a curved-beam under axial and bending strain. The proposed model relies upon the hypothesis of moderate curvature, which is certainly met in architectural applications where the radius of curvature is of the order of several meters, while glass thickness is just a few millimeters. This hypothesis allows simplifications in the governing equations that permit to define simple formulas for the deflection- and stress-effective thickness, representing a ready-to-use tool for the design of curved laminates. The shear coupling through the interlayer depends upon the stiffness of both glass and polymer, the geometric characteristics of the laminated package, the load and the boundary conditions. In the simplest cases, such as when the curvature is constant, the relevant parameters defining the effective thickness can be determined analytically. For more complicated conditions, a practical procedure is here proposed to readily calculate the effective thickness starting from a preliminary structural analysis, which can be performed with any commercial FEM code (not specific for laminates), or from simple experimental tests. Several paradigmatic examples are presented, for which comparisons with accurate 3D numerical experiments evidence the accuracy of the proposed approach.

2 Curved laminated beams

Consider a curved laminated beam of width b, composed of two external layers of the same thickness h, sandwiching a compliant thin interlayer of thickness $t \ll h$. The external layers are modeled as Euler-Bernoulli beams for which the classical assumption that plane cross sections remain plane and perpendicular to the longitudinal axis holds, whereas the interlayer has negligible axial and flexural stiffness, but provides the shear coupling of the external plies. As represented in Figure 1a, let us define the curvilinear abscissa s, parameterized by arc length with $0 \leq s \leq S$, lying in the middle surface of the whole beam, and the corresponding reference system formed by the tangent unit-vector $\mathbf{t}(s)$, positive in the direction of increasing s, and the normal unit-vector $\mathbf{n}(s)$, such that $\mathbf{n}(s) \times \mathbf{t}(s)$ is pointing outwards the plane of representation.

The geometric parameters are represented in Figure 1b. The external layers are labelled as "1" and "2" and both have the same Young's modulus E and Poisson's ratio ν, while the interlayer shear modulus is G. Therefore, the cross sectional area and the moment of inertia of each one of the external plies read

$$A = bh, \qquad I = \frac{bh^3}{12}. \tag{2.1}$$

Let then $R(s)$ denote the radius of curvature of the beam axis at s, with the notation that $R(s)$ is positive if the center of curvature is in the same direction of positive $\mathbf{n}(s)$. Denoting by $H = h + t$ the distance between the centroids of the cross sections of the external plies, the radius of curvature (with sign) of plies 1 and 2 are $R_1(s) = R(s) + H/2$ and $R_2(s) = R(s) - H/2$, respectively. Obviously, if $R(s) > 0$, $R_1(s) > R(s)$ and $R_2(s) < R(s)$, whereas in the opposite case $|R_1(s)| < |R(s)|$ and $|R_2(s)| > |R(s)|$.

The curvature is assumed *moderate*, i.e., the order parameter h/R is a quantity infinitesimal of the first order[1]. In general [9], as an order of magnitude, when $h/R < 1/10$ Navier's formula can be conveniently used to calculate the bending stresses in the curved beam, while the effects of curvature can be neglected when calculating the deflections when $h/R < 1/5$.

2.1 Kinematical assumptions

Under the hypothesis of moderate curvature, the tangential and normal unit vectors to the middle surface of layers "1" and "2" at s in practice coincide with $\mathbf{t}(s)$ and $\mathbf{n}(s)$, associated with the middle surface of the whole beam. If strains are infinitesimal and rotations are small, the kinematics is completely described by the displacement in the $\mathbf{n}(s)$ direction $v(s)$, the same for the whole laminated package, and the displacements in the $\mathbf{t}(s)$ direction $u_{01}(s)$ and $u_{02}(s)$ of the centroid of layers "1" and "2", respectively. Let then r_i denote the

[1] In the case of curved architectural glass this hypothesis is verified, because R is of the order of several meters, while h is of the order of a few millimeters.

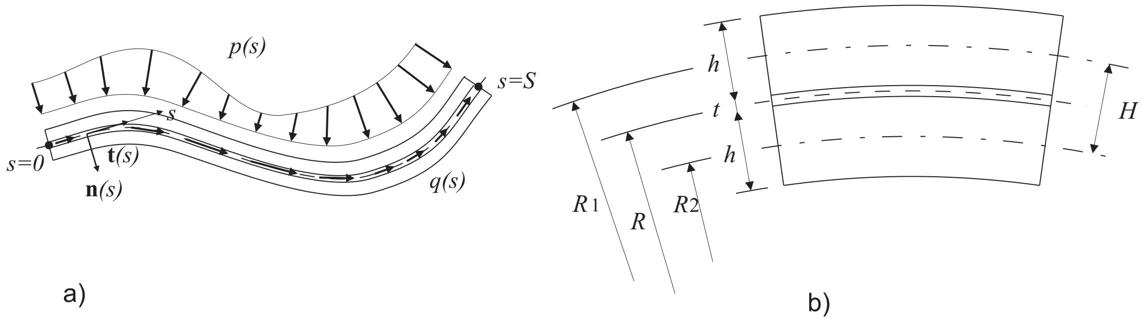

Figure 1: Curved sandwich beam: a) longitudinal view; b) Magnification of a beam voussoir.

distance of the generic point from the centroid of the $i-$th layer, measured in the direction of positive $\mathbf{n}(s)$, so that (s, r_i) represents a system of curvilinear coordinates for such layer. Following the classical Euler-Bernoulli's assumption, the displacement $\mathbf{u}_i(s, r_i)$ of the point (s, r_i), $i = 1, 2$, can be written as

$$\mathbf{u}_i(s, r_i) = [u_{0i}(s) + \phi_i(s) r_i]\mathbf{t}(s) + v(s)\mathbf{n}(s)\,, \tag{2.2}$$

where $\phi_i(s)$ is the rotation of the $i-$th cross section, considered positive if in the same direction of $\mathbf{n}(s) \times \mathbf{t}(s)$ according to the right-hand screw rule. Requiring that the shear component of the strain is null (see [22] for the details), one can demonstrate that $\phi_i(s) = -\Big[u_{0i}(s)/R(s) + v'(s)\Big]$, where $R(s)$ is the *signed* radius of curvature and, here and further, $(')$ denotes differentiation with respect to s.

Since the curvature is moderate, the normal component of strain in the $\mathbf{t}(s)$ direction of the $i-$th layer, $\varepsilon_{i;tt}(s, r_i)$, can be written in the form

$$\varepsilon_{i;tt}(s, r_i) = \varepsilon_{0i}(s) + \phi_i'(s) r_i\,, \qquad \varepsilon_{0i}(s) = u_{0i}'(s) - \frac{v(s)}{R(s)}\,, \tag{2.3}$$

where $\varepsilon_{0i}(s)$ is the normal component of strain at the centroid of the $i-$th layer, at $r_i = 0$.

Since the interlayer is thin, the component of strain in radial direction can be neglected. Moreover, due to the fact that the curvature is moderate, the shear component of strain $\gamma(s)$ can be assumed to be constant across the interlayer itself (see [22, 4]).

Referring to Figure 2, let $u_{sup}(s)$ and $u_{inf}(s)$ denote the horizontal displacement at the interface with the interlayer. One can find

$$\begin{cases} u_{sup}(s) = u_{01}(s) + \phi_1(s)\frac{h}{2} = u_{01}(s)\big(1 - \frac{h}{2R}\big) - v'(s)\frac{h}{2}\,, \\[2ex] u_{inf}(s) = u_{02}(s) - \phi_2(s)\frac{h}{2} = u_{02}(s)\big(1 + \frac{h}{2R}\big) + v'(s)\frac{h}{2}\,. \end{cases} \tag{2.4}$$

The shear strain in the interlayer is thus given by

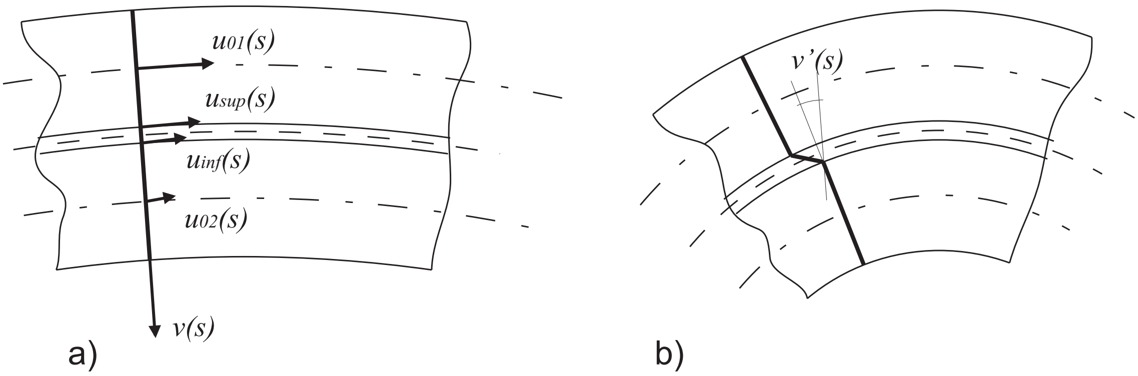

Figure 2: Relevant displacement components and corresponding deformation in the composite beam.

$$\gamma(s) = \frac{1}{t}[u_{inf}(s) - u_{sup}(s) + v'(s)t] = \frac{1}{t}\left[u_{02}(s)\left(1+\frac{h}{2R}\right) - u_{01}(s)\left(1-\frac{h}{2R}\right) + v'(s)H\right]. \quad (2.5)$$

Since the curvature is moderate, i.e., $h/R \ll 1$, terms of the type $\frac{h}{2R}$ may be neglected. In this case, the expression for $\gamma(s)$ coincides with that obtained for a straight sandwich beam found in [17].

2.2 Strain energy and governing equilibrium equations in the case of very small curvature

When the curvature is very small ($h/R < 10^{-2}$), the axial strain and the rotation may be simplified in the form

$$\varepsilon_{0i}(s) = u'_{0i}(s) - \frac{v(s)}{R} \simeq u'_{0i}(s), \qquad \phi_i(s) = -\left[\frac{u_{0i}(s)}{R} + v'(s)\right] \simeq -v'(s). \quad (2.6)$$

The major consequence is that the axial and flexural response of the beam are not coupled. In fact, the bending moment $M_i(s)$ and the axial force $N_i(s)$ acting on the i−th layer are related only to the radial and the tangential displacement, respectively, in the form

$$M_i(s) = EI\phi'_i(s) \simeq -EIv''(s), \qquad N_i(s) = EA\varepsilon_{0i}(s) \simeq EAu'_{0i}(s). \quad (2.7)$$

This leads to noteworthy simplifications.

It is useful to introduce the fields

$$u_+(s) := \frac{u_{01}(s) + u_{02}(s)}{2}, \qquad u_-(s) := \frac{u_{01}(s) - u_{02}(s)}{2}, \quad (2.8)$$

where $u_+(s)$ may be regarded as the mean tangential displacement of the composite beam, which is associated with the total axial force acting on the whole laminated package because

$$N(s) := N_1(s) + N_2(s) = 2EAu'_+(s)\,. \tag{2.9}$$

Hence, the shear strain in the interlayer $\gamma(s)$ of (2.5) and the corresponding shear force per unit length transmitted by the interlayer $\tau(s)$ can be written as

$$\gamma(s) = \frac{1}{t}[-2u_-(s) + v'(s)H]\,, \qquad \tau(s) = Gb\gamma(s) = \frac{Gb}{t}[-2u_-(s) + v'(s)H]\,. \tag{2.10}$$

Therefore, the energy functional can be written as a function of the displacement fields $v(s)$, $u_+(s)$ and $u_-(s)$ in the form

$$\begin{aligned}\mathfrak{E}[u_+(s), u_-(s), v(s)] = \int_0^S \Big\{ & EA[(u'_+(s))^2 + (u'_-(s))^2] + EI(v''(s))^2 \\ & + \frac{Gb}{2t}[-2u_-(s) + v'(s)H]^2 - [p(s)\ v(s) + q(s)\ u_+(s)]\Big\} ds\,, \end{aligned} \tag{2.11}$$

where the first and the second terms represent the extensional and the flexional contribution of the upper and lower external plies, respectively, while the third term is the strain energy due to the shear elastic strain of the interlayer. The last term expresses the contribution of the radial and tangential external loading $p(s)$ and $q(s)$.

The zeroing of the first variation of the functional with respect to the variations of $v(s)$, $u_+(s)$ and $u_-(s)$ gives, respectively, the following Euler's equilibrium equations

$$2EIv''''(s) - \frac{GbH}{t}[-2u_-(s) + v'(s)H]' - p(s) = 0\,, \tag{2.12}$$

$$2EAu''_+(s) + q(s) = 0\,, \tag{2.13}$$

$$2EAu''_-(s) + \frac{2Gb}{t}[-2u_-(s) + v'(s)H] = 0\,. \tag{2.14}$$

To give a physical interpretation of these equations, as shown in Figure 3 imagine to cut the interlayer at an arbitrary level t^* and observe that the shear force (per unit length) $\tau(s)$ transmitted by the interlayer produces a distributed couple per unit length $m_1(s) = -\tau(s)(h/2 + t^*)$ in layer "1" and $m_2(s) = -\tau(s)(h/2 + t - t^*)$ in layer "2". Therefore, recalling $(2.10)_2$, equation (2.12) represents the radial equilibrium of a beam with moment of inertia $2I$, under a distributed radial load $p(s)$ and a distributed couple per unit length $m(s) = m_1(s) + m_2(s) = -\tau(s)H$, i.e., $2EIv''''(s) + m'(s) - p(s) = 0$ [36, 35].

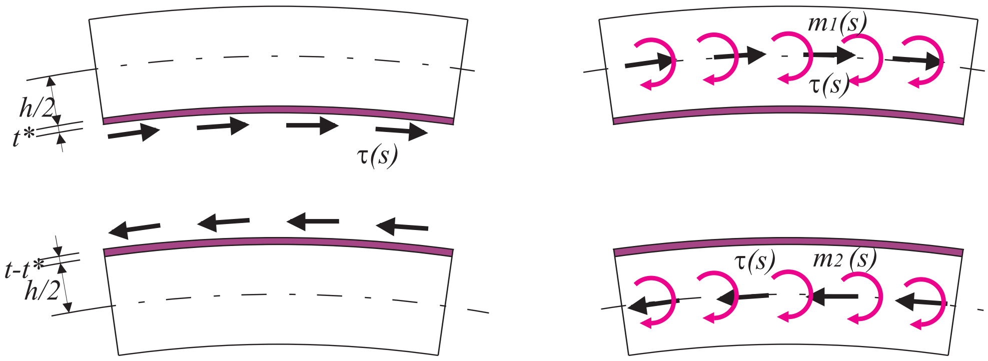

Figure 3: Effect of the shear force per unit length transmitted by the interlayer.

In terms of the bending moments and axial forces defined by (2.7), equations (2.12), (2.13) and (2.14) may be re-written as

$$-M_1''(s) - M_2''(s) + m'(s) - p(s) = 0\,, \tag{2.15}$$
$$N_1'(s) + N_2'(s) + q(s) = 0\,, \tag{2.16}$$
$$N_1'(s) - N_2'(s) + 2\tau(s) = 0\,. \tag{2.17}$$

Equation (2.13) (or, equivalently, (2.16)) represents the equilibrium in tangential direction of a beam with area $2A$, under the distributed tangential load $q(s)$. The total axial force acting on the beam is given by (2.9). Moreover, equation (2.14), or equivalently (2.17), relates the difference between the axial forces acting on the glass plies, equal to $2EAu_-''(s)$, to the shear force per unit length transmitted across the interlayer. Notice that in all these equations the effect of curvature is considered negligible.

Standard arguments in the calculus of variation [34] furnish the following boundary conditions

$$\begin{aligned}
&\Big[(-2EIv'''(s) + GbH\gamma(s))\delta v(s)\Big]_0^S = 0\,,\\
&\Big[2EIv''(s)\delta v'(s)\Big]_0^S = 0\,,\\
&\Big[2EAu_+'(s)\delta u_+(s)\Big]_0^S = 0\,,\\
&\Big[2EAu_-'(s)\delta u_-(s)\Big]_0^S = 0\,,
\end{aligned} \tag{2.18}$$

where $\delta v(s)$, $\delta u_+(s)$ and $\delta u_-(s)$ denote the variations of $v(s)$, $u_+(s)$ and $u_-(s)$. Such variations are null at the boundary where the displacement is prescribed, and arbitrary otherwise. Observe, in particular, that the quantity $-2EIv'''(s)+GbH\gamma(s)$ plays the role of the total shear force acting on the composite beam.

2.3 Layered and monolithic limits

The layered and monolithic limits correspond, respectively, to the borderline cases of evanescent stiffness of the interlayer (frictionless sliding external plies), and shear-stiff interlayer (no relative slip between the glass plies).

The equilibrium equations for the *layered limit* are obtained by setting $G=0$. Equations (2.12), (2.13) and (2.14) thus become

$$\begin{aligned} &EI_L\, v_L''''(s)-p(s)=0\,,\\ &u''_{+L}(s)=-\frac{q(s)}{2EA}\,,\\ &u''_{-L}(s)=0\,, \end{aligned} \tag{2.19}$$

where the suffix L evidences that the displacement field refers to the layered limit. These correspond to the equilibrium of two frictionless sliding glass beams with moment of inertia $I_L=2I$ and area $2A$. The third of (2.19) indicates that $2EAu'_{-L}(s)=N_1(s)-N_2(s)$ is constant in $0\le s\le S$. But if at one of the extremities $s=0$ or $s=S$, the applied external forces are such that $N_1=N_2$, i.e., the applied axial force is equally divided into the constituting layers, then $N_1(s)=N_2(s)\ \forall s$. Moreover, in order to avoid undefined sliding of the two external layers, one can impose that $u_{-L}(s_1)=0$ at one point s_1. This implies that $u_{-L}(s)=0\ \forall s$ and, consequently from $(2.8)_2$, that $u_{01}(s)=u_{02}(s)\Rightarrow u_{+L}(s)=0$.

When $G\to\infty$ (monolithic limit), a relationship between tangential and radial displacement can be obtained by imposing that the shear strain $\gamma(s)$, defined by (2.5), is null. From equation (2.14) this allows to obtain $\tau(s)=-EAu''_{-}(s)=-\frac{EAH}{2}v'''(s)$. Consequently, (2.12), (2.13) and (2.14) become

$$\begin{aligned} &EI_M\, v_M''''(s)-p(s)=0\,,\\ &u''_{+M}(s)=-\frac{q(s)}{2EA}\,,\\ &u_{-M}(s)=\frac{H}{2}v'_M(s)\,, \end{aligned} \tag{2.20}$$

where now the suffix M denotes reference to the monolithic limit and $I_M=2I+AH^2/2$ is the moment of inertia of the composite beam whenever the monolithic limit is attained [17], i.e., the inertia of the two external layers properly spaced of the gap given by the thickness of the interlayer.

The boundary conditions for $u_{+M}(s)$ and $u_{+L}(s)$ at $s = 0$ and $s = S$ are given by expressions analogous to $(2.18)_3$. Therefore, from $(2.19)_2$ and $(2.20)_2$, one has that $u_{+M}(s) = u_{+L}(s)$ and such fields are governed by the tangential component $q(s)$ only of the applied load, and not by the radial component $p(s)$. In general one can set $u_+(s) = u_{+L}(s) = u_{+M}(s)$. This means that the mean tangential displacement, as well as the total axial force $N(s)$ given by (2.9), are not influenced by the degree of shear coupling offered by the interlayer.

3 Enhanced Effective Thickness Approach

The deflection- and stress-effective thickness of laminated glass is the (constant) thickness of a monolith that, under the same boundary and load conditions, presents the same maximum deflection or maximum stress, respectively. As explained in [17, 19, 24], the Enhanced Effective Thickness approach consists in finding the best approximation for for the deflection surface of laminated glass among a restricted class of shape functions, associated with the minimization of the strain energy functional.

3.1 Basic assumptions and strain energy functional

The strain energy functional that will be considered is a slight generalization of the expression presented in Section 2.2. In fact, equation (2.13), or equivalently (2.16), is not accurate unless the beam is “almost straight”, because in general the axial force depends not only upon the tangential load, but also on the curvature. Nevertheless, the uncoupling of the extensional and flexural response is a crucial assumption for the forthcoming deductions.

The hypotheses that will be considered here are the followings.

i. The radial displacement field $v(s)$ is a linear combination of the fields $v_L(s)$, associated with the layered limit ($G = 0$), and $v_M(s)$, corresponding to the monolithic limit ($G \to \infty$), i.e.,

$$v(s) = (1 - \eta)\ v_L(s) + \eta\ v_M(s)\ . \tag{3.1}$$

ii. The skew part of the tangential displacement fields $u_-(s)$ is compatible with equations $(2.19)_3$ (layered limit) and $(2.20)_3$ (monolithic limit), and is again a linear combination of the two corresponding fields. Therefore, it is of the form

$$u_-(s) = (1 - \eta)\ u_{-L}(s) + \eta\ u_{-M}(s) = \eta \frac{H}{2} v'_M(s)\,. \tag{3.2}$$

iii. The mean tangential displacement fields $u_+(s)$ is again a linear combination of the layered and monolithic limits, i.e., it is of the form

$$u_+(s) = (1-\eta)\; u_{+L}(s) + \eta\; u_{+M}(s)\,. \tag{3.3}$$

iv. The mean axial strain in the beam, here referred to as $\varepsilon_+(s)$, is *independent* of the shear coupling offered by the interlayer, and the corresponding total axial force is given by

$$N(s) = 2EA\varepsilon_+(s)\,. \tag{3.4}$$

This assumption is more general than that corresponding to (2.9), because the mean axial strain is not any longer associated with the tangential derivative of $u_+(s)$, and such field is not necessarily related with the sole radial component of the load $q(s)$ as per (2.13) and (2.16). In other words, the expressions of the mean axial strain and axial force in the beam can now take into account the geometric effects of the curvature, but we are still maintaining the hypothesis that the flexural properties of the layered package are independent from its axial properties.

The resulting class of shape functions is certainly compatible with the qualitative properties of the exact solution, in particular with the prescribed boundary conditions. The quantity η is clearly a non-dimensional *shear coupling parameter*, tuning the behavior from the layered limit ($\eta = 0$) to the monolithic limit ($\eta = 1$). The radial displacement fields $v_L(s)$ and $v_M(s)$, as well as $u_{+L}(s)$ and $u_{+M}(s)$, are to be regarded as known, because they can be determined by solving the elastic problem of the curved beam under assigned loads and boundary conditions, whose cross sectional area is $2A$ and the moment of inertia is, respectively, equal to $I_L = 2\,I$, or $I_M = 2\,I + AH^2/2$. The mean axial strain $\varepsilon_+(s)$ derives from the constitute equation $N = 2\,EA\,\varepsilon_+(s)$ and is definitely known; remarkably, it is *independent* of the shear coupling of the laminated package, if the beam is statically determined. The approximation consists in assuming that such independence is always true, even when the constraints in the beam are redundant.

The total energy (2.11) thus becomes a function of the parameter η only and can be written in the form

$$\begin{aligned}\widetilde{\mathfrak{E}}^*[\eta] = \int_0^S \Big\{ & EA\,(\varepsilon_+(s))^2 + \frac{EAH^2}{4}\eta^2\left(v''_M(s)\right)^2 \\ & + EI\left[(1-\eta)v''_L(s) + \eta\; v''_M(s)\right]^2 + \frac{Gb}{2t}\left[(1-\eta)v'_L(s)H\right]^2 \\ & - p(s)\left[(1-\eta)v_L(s) + \eta\; v_M(s)\right] - q(s)\left[(1-\eta)\; u_{+L}(s) + \eta\; u_{+M}(s)\right]\Big\} ds\,.\end{aligned} \tag{3.5}$$

This expression can be simplified by writing two virtual work equalities for a system in which the applied external loads are $p(s)$ and $q(s)$, while the stress and displacement fields are those associated with either the layered or the monolithic solutions. Therefore, substituting

$$\begin{aligned}
\int_0^S [p(s)v_L(s) + q(s)u_{+L}(s)]\ ds &= EI_L \int_0^S (v_L''(s))^2\ ds + 2EA \int_0^S (\varepsilon_+(s))^2\ ds\,, \\
\int_0^S [p(s)v_M(s) + q(s)u_{+M}(s)]\ ds &= EI_M \int_0^S (v_M''(s))^2\ ds + 2EA \int_0^S (\varepsilon_+(s))^2\ ds\,,
\end{aligned} \tag{3.6}$$

into (3.7), one finds

$$\begin{aligned}
\widetilde{\mathfrak{E}}[\eta] = {} & EA \int_0^S (\varepsilon_+(s))^2\ ds + \frac{EAH^2\eta^2}{4} \int_0^S (v_M''(s))^2\ ds \\
& + \frac{EI_L}{2} \int_0^S [(1-\eta)v_L''(s) + \eta v_M''(s)]^2\ ds + \frac{Gb(1-\eta)^2H^2}{2t} \int_0^S (v_L'(s))^2\ ds \\
& - EI_L(1-\eta) \int_0^S \left(v_L''(s)\right)^2\ ds - EI_M\eta \int_0^S \left(v_M''(s)\right)^2\ ds - 2EA \int_0^S (\varepsilon_+(s))^2\ ds.
\end{aligned} \tag{3.7}$$

Its minimization with respect to parameter η leads to the following linear algebraic equation

$$\begin{aligned}
& \frac{EAH^2}{2}\eta \int_0^S (v_M''(s))^2\ ds \\
& \quad + EI_L\Big[-(1-\eta) \int_0^S (v_L''(s))^2\ ds + \eta \int_0^S (v_M''(s))^2\ ds + (1-2\eta) \int_0^S v_M''(s)v_L''(s)\ ds \Big] \\
& - \frac{GbH^2}{t}(1-\eta) \int_0^S \left(v_L'(s)\right)^2\ ds + EI_L \int_0^S (v_L''(s))^2\ ds - EI_M \int_0^S (v_M''(s))^2\ ds = 0\ .
\end{aligned} \tag{3.8}$$

The solution of this equation represents the value of η that defines the deformation of the beam in the assumed class of shape functions.

3.2 The class of shape functions

Further simplifications are possible by exploiting further the consequences of the assumption that the field $\varepsilon_+(s)$ does not depend upon the shear coupling of the laminated package. Consider now the Virtual Work equalities for a system in which the force/stress field is the one corresponding to the monolithic limit and the displacement/strain field is that associated with the layered limit, and viceversa. Since the applied forces are $p(s)$ and $q(s)$ in both cases, one obtains

$$
\begin{aligned}
&\int_0^S [p(s)v_L(s)+q(s)u_{+L}(s)]\,ds = EI_M\int_0^S v_L''(s)v_M''(s)\;ds + 2EA\int_0^S (\varepsilon_+(s))^2\;ds\,,\\
&\int_0^S [p(s)v_M(s)+q(s)u_{+M}(s)]\,ds = EI_L\int_0^S v_L''(s)v_M''(s)\;ds + 2EA\int_0^S (\varepsilon_+(s))^2\;ds\,.
\end{aligned}
\tag{3.9}
$$

Notice that the last term in all these expressions is the same because of the hypothesis that the main axial strain is independent of the shear coupling through the interlayer.

Re-arranging equations (3.6) and (3.9), one finds

$$
\begin{aligned}
&\int_0^S [p(s)\,(v_M(s)-v_L(s)) + q(s)\,(u_{+M}(s)-u_{+L}(s))]\,ds\\
&\qquad = E\Big[I_M\int_0^S (v_M''(s))^2\;ds - I_L\int_0^S (v_L''(s))^2\;ds\Big]\\
&\qquad = E[I_L - I_M]\int_0^S v_L''(s)v_M''(s)\,ds\,.
\end{aligned}
\tag{3.10}
$$

Remarkably, this expression is satisfied if the radial displacement fields corresponding to the layered and monolithic limit, i.e., $v_L(s)$ and $v_M(s)$, are inversely proportional to the corresponding moment of inertia, I_L and I_M. In other words, depending upon the geometry, the applied loads and boundary conditions of the beam, a function $g(s)$ exists such that

$$
v_L(s)=\frac{g(s)}{EI_L}\,,\qquad v_M(s)=\frac{g(s)}{EI_M}\,. \tag{3.11}
$$

This means that the *form* of the deformed shape is also independent of the shear coupling through the interlayer: it is determined by the geometry, as well as by loading and boundary conditions. The radial displacement field is evaluated through equation (3.1), which, according to (3.11), can be written in the form

$$
v(s)=\frac{g(s)}{EI_{eq}}\,,\qquad \frac{1}{I_{eq}} := \frac{1-\eta}{I_L}+\frac{\eta}{I_M}\,. \tag{3.12}
$$

Thus, I_{eq} may be regarded as the effective moment of inertia of the laminated glass beam, i.e., the moment of inertia of the monolith that presents the same deflection. Remarkably, in the proposed approach I_{eq} is the weighted harmonic mean, through the parameter η, of the moments of inertia corresponding to the layered and monolithic limits.

3.3 The Enhanced Effective Thickness for displacement and stress

The solution of equation (3.8), taking into account (3.11), is

$$\frac{1}{\eta} = 1 + \frac{Et}{2\,Gb}\frac{I_L}{I_M}\frac{A\ \int_0^S (g''(s))^2\ ds}{\int_0^S (g'(s))^2\ ds}\,. \tag{3.13}$$

Observe that the shear coupling coefficient η depends upon the mechanical properties of both glass and interlayer, on the geometry of the beam, as well as on the boundary and loading conditions. In particular, at the monolithic limit $G \to \infty \ \Rightarrow \eta = 1$, whereas at layered limit $G = 0 \ \Rightarrow \eta \to 0$. Expression (3.13) formally coincides with the shear coupling coefficient determined in [17] for the case straight laminated glass beam. However, expression (3.13) does not depend upon the beam curvature only apparently, because the shape function $g(s)$, defined through (3.11), is the radial displacement field of the beam under consideration, which is certainly influenced by the beam curvature.

By introducing a non dimensional abscissa $x := (2s/S - 1)\,,\ x \in [-1, 1]$, expression (3.13) may be rearranged as

$$\frac{1}{\eta} = 1 + \frac{2Et}{Gb}\frac{I_L}{I_M}\frac{A}{S^2}\Upsilon\,, \qquad \Upsilon = \frac{\int_{-1}^{1} (g_{,xx}(x))^2\ dx}{\int_{-1}^{1} (g_{,x}(x))^2\ dx}\,, \tag{3.14}$$

where comma denotes differentiation with respect to the indicated variable and Υ is a non dimensional parameter, where the influence of loading and geometry of the beam is enclosed.

The parameter η can be used to define the *deflection-effective thickness* $\hat{h}_w$, i.e., the thickness of a monolithic beam having the same deflection of the laminated beam. Equating the moments of inertia as per (3.12), one finds

$$\frac{1}{\hat{h}_w} = \sqrt[3]{\frac{\eta}{2h^3 + 6hH^2} + \frac{1-\eta}{2h^3}}\,. \tag{3.15}$$

Furthermore, reasoning as in [17], one finds that the *stress-effective thickness* $\hat{h}_\sigma$, i.e., the thickness of a monolith that presents the same maximum stress of the laminated beam, reads

$$\hat{h}_\sigma = \sqrt{\frac{\eta\,H}{2h^3 + 6hH^2} + \frac{h}{\hat{h}_w^3}}\,. \tag{3.16}$$

The importance of such expressions consists in the fact that a designer can calculate the deflection and stress in a laminated glass elements using the structural methods for elastic monolithic beams, through the equivalence established by (3.15) and (3.16). The parameter η will be calculated in the following sections for the cases of most practical interest.

3.4 Other proposed expressions for the effective thickness

To our knowledge, no other specific approaches to calculate the effective thickness of curved laminated glass have been proposed so far. However, in the case of moderate curvature, some authors have suggested to use the same formulas proposed for straight beams.

In particular, a classical approach is based upon the model originally proposed by Wölfel [37] and later developed by Bennison et al. [10, 7]. Such method is adopted by the American standard ASTM-E1300 [30] and relies upon several simplifying assumptions that, as discussed detail in [17], render it accurate for the case of simply supported beams under uniformly distributed loading.

According to the Wölfel-Bennison method, with the same notation of the previous sections, the *deflection-effective thickness* $h_{w;WB}$ and the *stress-effective thickness* $h_{\sigma;WB}$ of a laminated glass beam of length l is determined by

$$h_{w;WB} = \sqrt[3]{2h^3 + 6\Gamma h H^2} \qquad h_{\sigma;WB} = \sqrt{\frac{h^3_{w;WB}}{h + \Gamma H}} \tag{3.17}$$

where Γ is the shear coupling parameter, given by

$$\Gamma = \frac{1}{1 + 9.6 \frac{Et}{Gbl^2} \frac{A}{2}} \,. \tag{3.18}$$

For the case of curved beams, it is reasonable to consider the beam length l equal to the arc length S.

In order to evaluate the accuracy of the EET method, it will be applied in following sections to arches with different geometries, boundary and loading condition, making comparisons with results obtainable from the Wölfel-Bennison method and from accurate numerical experiments.

4 Examples: beams with constant curvature

Consider a curved beam with constant radius of curvature $R(s) = R = \ const.$ The total energy of the system (2.11) may be written as a function of the angular variable $\theta = s/R$, $\theta \in [\Theta_1, \Theta_2]$, so that the shear coupling coefficient η of (3.13) reads

$$\frac{1}{\eta} = 1 + \frac{Et}{2Gb} \frac{I_L}{I_M} \frac{A}{R^2} \Upsilon_\theta \,, \qquad \Upsilon_\theta = \frac{\int_{\Theta_1}^{\Theta_2} (\hat{g},_{\theta\theta}(\theta))^2 \, d\theta}{\int_{\Theta_1}^{\Theta_2} (\hat{g},_{\theta}(\theta))^2 \, d\theta} \,, \tag{4.1}$$

where $\hat{g}(\theta)$ is the shape function for the vertical displacement in terms of the variable θ.

In the example of Figure 4a, the arch $-\Theta \leq \theta \leq \Theta$, of width $b = 1$ m and radius of curvature R, is composed by two external glass plies of thickness $h = 10$ mm and Young's modulus $E = 70000$ MPa, sandwiching an interlayer of thickness $t = 0.76$ mm, whose shear modulus G is varied in the range $[10^{-3} \div 10]$ MPa, in order to evaluate its influence on the shear-coupling of the external plies.

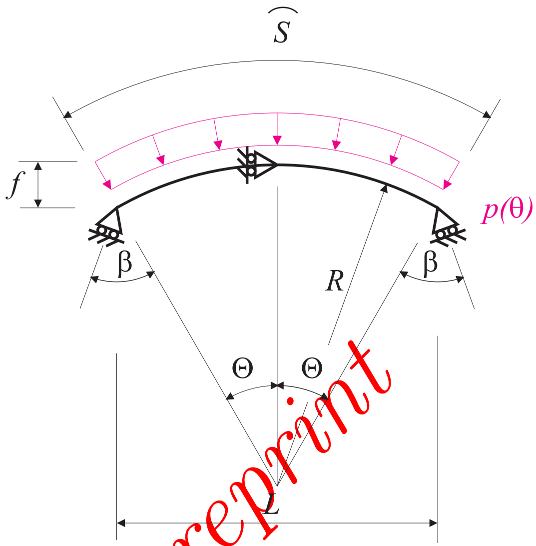

Figure 4: Geometric definition of an arch beam of laminated glass with constant curvature.

The distributed tangential force *per* unit length is null ($q = 0$), whereas the pressure (in radial direction) is equal to 0.75 kN/m^2, so that the corresponding load *per* unit length is $p(\theta) = p_0 = 0.75$ N/mm. The arch span is $L = 2R\sin(\Theta)$, the arc length is $S = 2R\Theta$, while the rise is $f = R(1 - \cos(\Theta))$. The reference geometry is represented by $L = 3000$ mm, $f = 250$ mm, $S = 3217.5$ mm, $R = 2500$ mm, $\Theta = 36.87°$, but the geometrical parameters will be varied, in order to evaluate their influence.

Using the EET approach, FEM analyses have been performed on the monolithic arch with equivalent bending properties, defined through expressions (3.15) and (3.16). For the sake of comparison, numerical experiments have been made with the FEM code Abaqus, using a 3-D mesh with solid 20-node quadratic bricks with reduced integration, available in the program library [1], to provide a linear distribution of stress and strain within the element, compatibly with Euler-Bernoulli beam theory. The mesh, shown in Figure 5, has been created by dividing the length of the beam in 100 elements, its width in 30 elements and the thickness of each glass layer in 3 elements. No comparison with the Wölfel-Bennison approach is recorded because, for the case at hand, it furnishes values of effective thicknesses very close to those obtained with the EET approach, with differences of the order of 0.3%.

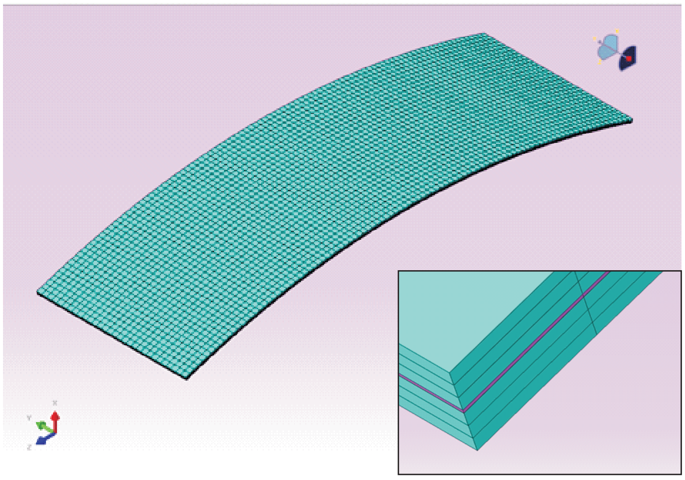

Figure 5: Mesh used in the FEM experiments.

4.1 Example A. Radial constraints

Consider the case $\beta = 0$ in Figure 4, i.e., the roller constraints are radial. The shape function for the radial displacement and, hence, the shear coupling coefficient Υ_θ of (4.1) can be evaluated analytically: the bending moment comes directly from equilibrium equations [9] and the shape function can be determined through $(2.7)_1$, with the corresponding boundary conditions. The shear coupling coefficient η and the *deflection-* and *stress-effective thickness* can thus be determined with (4.1), (3.15) and (3.16), respectively.

4.1.1 Effect of the rise/span ratio

The span of the laminated glass arch is kept fixed to $L = 3000$ mm, while the rise f is varied. Figure 6 shows the deflection- and stress-effective thickness for values of the rise f varying from 0 (corresponding to the limit case of straight beam) to 1000 mm, as a function of the shear modulus of the interlayer G in the interval from 10^{-3} MPa to 10 MPa. Such values are comprised between the layered limit ($G = 0$) and the monolithic limit ($G \to \infty$).

It is evident from the graphs that the lower is f (and, consequently, the lower is the arc length S), the lower is the effective thickness. This confirms what observed in [21] for straight beams, i.e., that for fixed G, the more slender is the laminated glass beam, the higher is the coupling offered by the interlayer.

The comparison, in terms of maximum radial deflection and maximum stress, of the results obtained with the EET approach and with 3D FEM analysis are presented in Figure 7. There is a very good agreement because the maximum error is of the order of 2%.

Graphs in Figure 8 show the effective thicknesses for arches whose length is fixed and equal to $S = 3217.5$ mm, while the radius of curvature R and, consequently, the angle Θ,

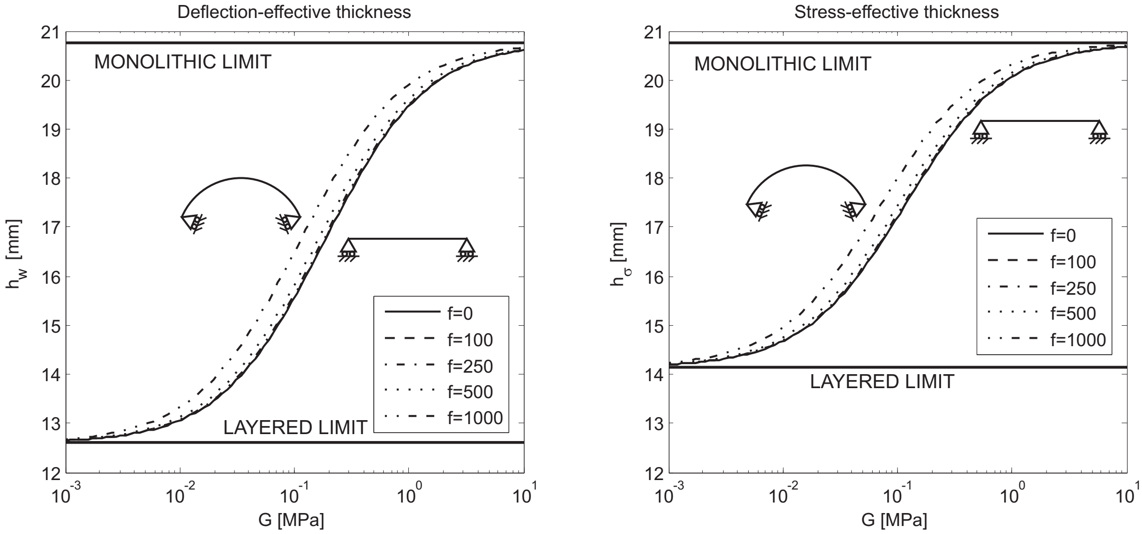

Figure 6: Arch with constant curvature under uniformly distributed radial load and radial constraints. Deflection- and stress-effective thickness for different values of the rise/span ratio.

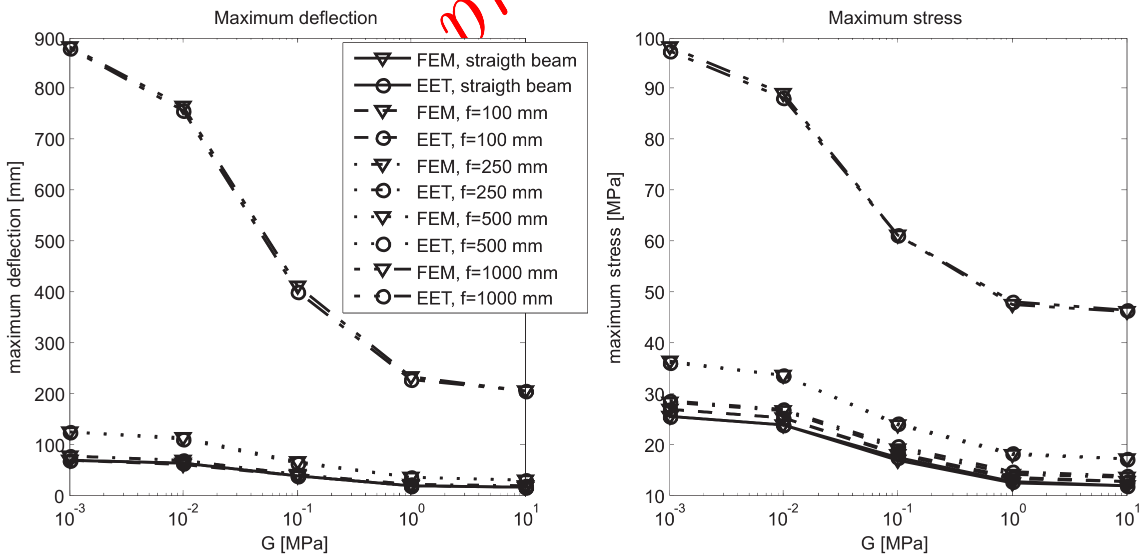

Figure 7: Arch with constant curvature and radial constrains, under uniformly distributed radial load. Comparison of maximum deflection and maximum stress evaluated with the EET model and a 3D FEM analysis, for different values of the rise f.

is varied. Observe that, in practice, all the graphs coincide. A comparison with Figure 7 remarkably indicates that, for fixed loading and boundary condition, the leading geometric governing parameter of shear-coupling through the interlayer is the arc length S, rather then the radius of curvature.

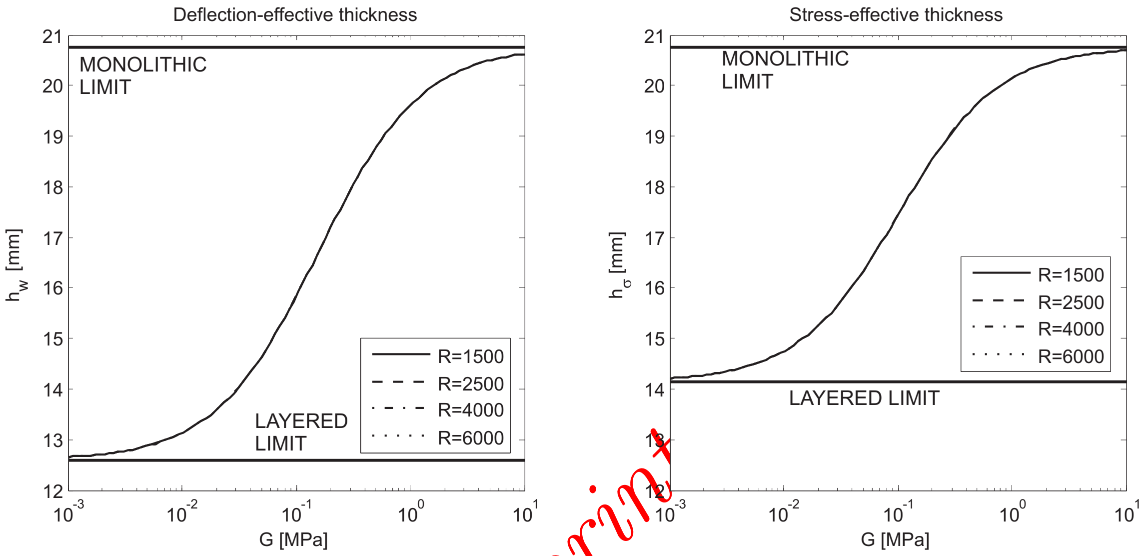

Figure 8: Circular arch with radial constraints under uniformly distributed radial load. Deflection- and stress-effective thickness for different values of the radius of curvature, for a given arc length.

4.1.2 Effect of the span/thickness ratio

In the circular arch the rise/span ratio is now kept fixed to $f/L = 1/12$ so that $\Theta = 36.87°$. Fixing $h = 10$ mm and $t = 0.76$ mm, the span L is varied.

Figure 9 shows the deflection- and stress-effective thickness, as a function of the shear modulus of the interlayer G, for values of ratio $L/2h$ comprised between 300 ($L = 6000$ mm) and 18.75 ($L = 375$ mm). Observe that, in agreement with the case of Section 4.1.1, the lower is the arc length, the lower is the shear coupling effect from the interlayer.

Figure 10 shows, as a function of the shear modulus of the interlayer G and for different values of the ratio $L/2h$, the maximum deflection and the maximum stress evaluated either with the EET method, or the 3D FEM analysis.

Figure 11 indicates, as a function of G, the mean percentage error obtained with the EET approach while evaluating the maximum deflection and stress, for different values of the span/thickness ratio. As expected, the accuracy of the proposed model decreases proportionally to $L/2h$. In other words, the EET method is accurate for arches with moderate curvature. In any case, for all the case of practical interest, for which certainly

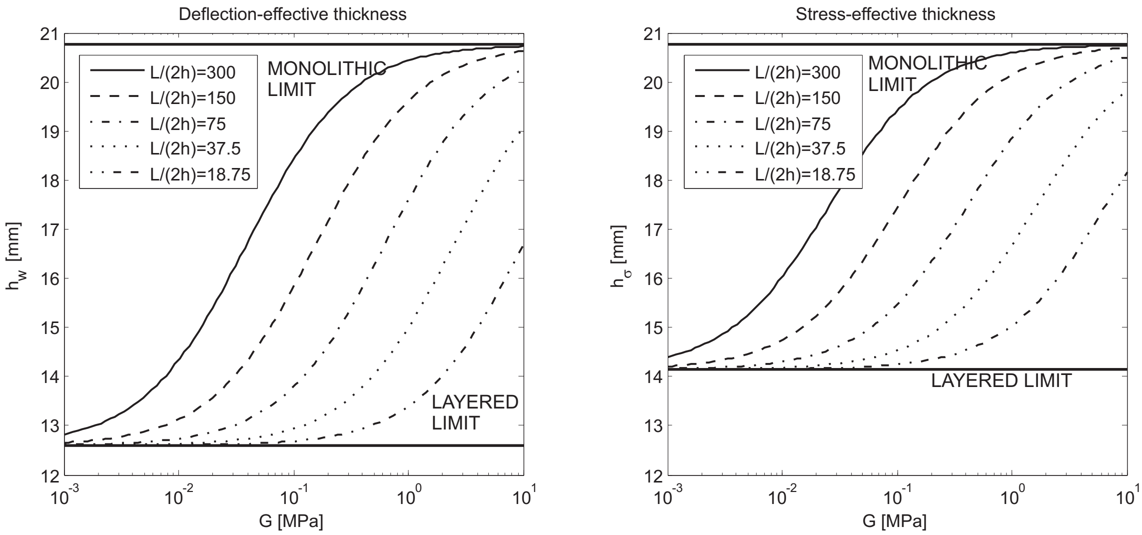

Figure 9: Circular arch with radial constraint, under uniformly distributed radial load. Deflection- and stress-effective thickness for different values of the span/thickness ratio.

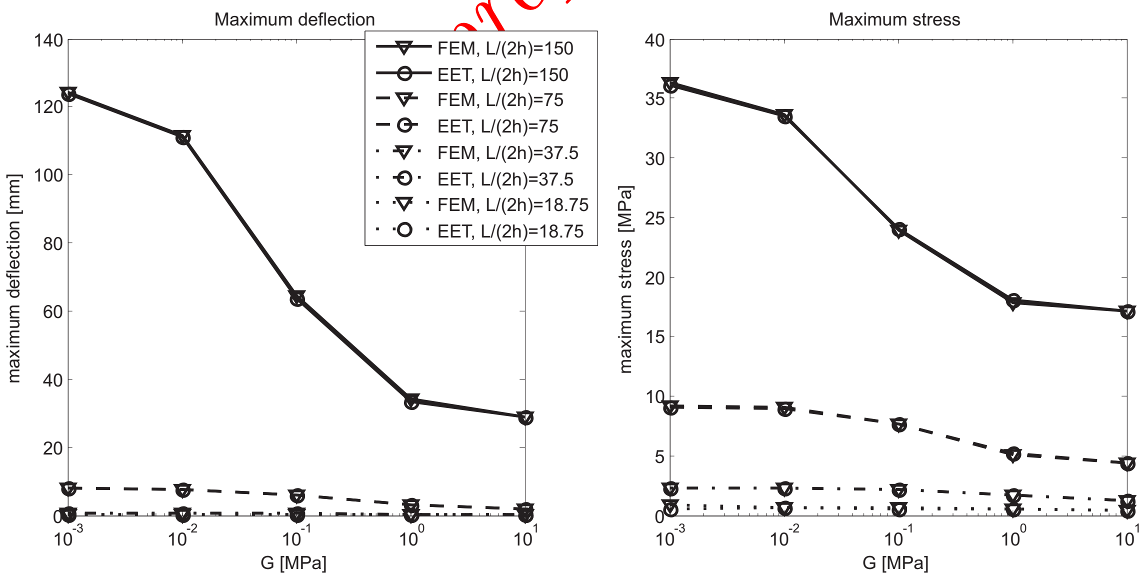

Figure 10: Circular arch with radial constraints, under uniformly distributed radial load. Comparison of maximum deflection and maximum stress evaluated with the EET model and the 3D FEM analysis, for different values of the span/thickness ratio.

$L/2h > 50$, the proposed approach turns out to be very reliable, with a mean error of the order of less than 1%.

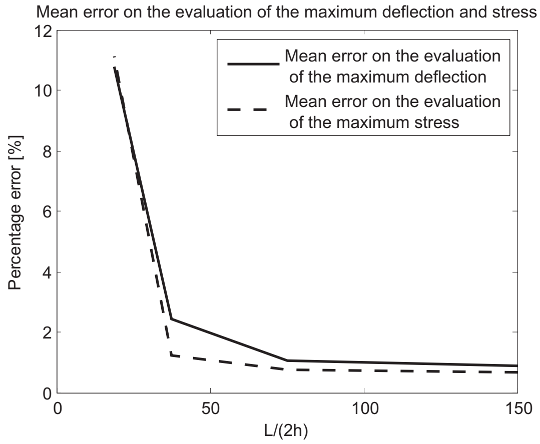

Figure 11: Circular arch with radial constraints, under uniformly distributed radial load. Mean percentage error in the evaluation of the maximum deflection and the maximum stress with the EET method, as a function of the span/thickness ratio.

4.2 Example B. Vertical constraints

In the structure of Figure 4 now set $\beta = \Theta$, so that the roller constraints prevents the vertical displacement. Observe that the constraint reaction can be decomposed into a radial and a tangential component. The static state of the system is obtained by superimposing two configurations: 1) the tangential component of the constraints reactions, which equilibrate a percentage of the applied load; 2) the radial components that equilibrates the remaining part of the applied loads. But it is well known that the system 1) provokes the axial contraction of the arch with no bending. Consequently, the flexural response is associated with the system 2) only. Therefore the shape function $g(\theta)$ to be used in equation $(4.1)_2$ coincides with the one calculated for Example A, and the deflection- and stress-effective thickness are the same.

It is however to be expected that the errors in the proposed EET method are greater than in the previous example, because the method does not consider the coupling between the axial and bending response of the sandwich beam, and the axial forces in Example B are much greater than in example A.

4.2.1 Effect of the rise/span ratio

For the same geometry and material properties of Section 4.1.1, since the shape function is equal to that of Example A, the graphs of the deflection- and stress-effective thickness as a function of G coincide with those of Figure 6.

Figure 12 is the counterpart of Figure 7, and shows the comparison of FEM analysis with results from the EET model. Despite the approximations of the model, results obtained with the EET approach are in good agreement with the numerical experiments, being the maximum error of 3%.

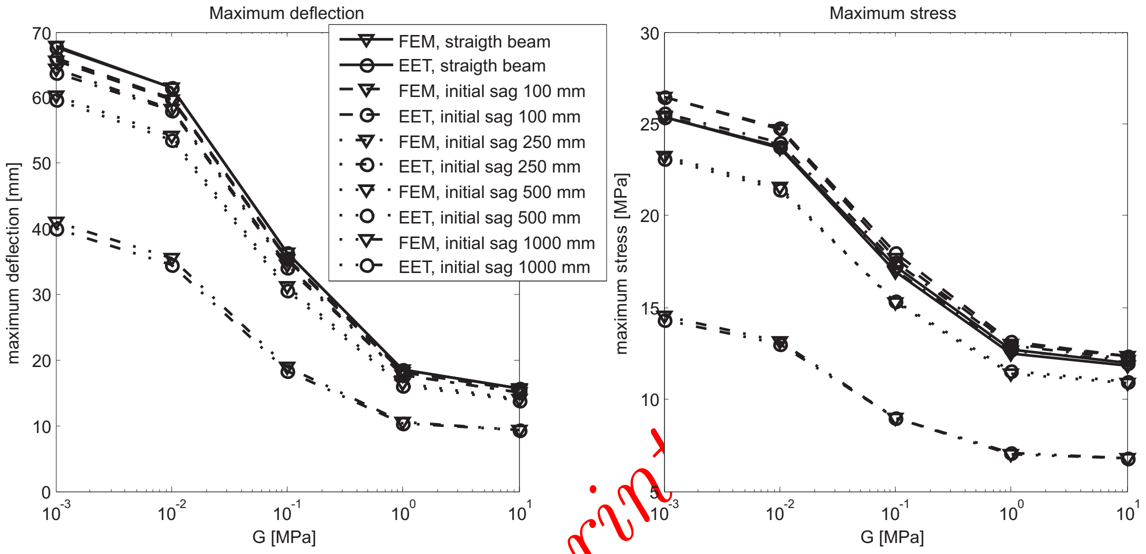

Figure 12: Circular arch with vertical constrains, under uniformly distributed radial load. Comparison of maximum deflection and maximum stress evaluated with the EET model and the 3D FEM analysis, for different values of the rise f.

4.2.2 Effect of the span/thickness ratio

In analogy with the analysis of Section 4.1.2, Figure 13 represents the counterpart of Figure 9, showing the maximum deflection and the maximum stress as functions of G for different value of $L/2h$, evaluated through the 3D numerical analysis and the EET method.

Figure 14 shows the mean percentage error (for the considered values of G) as a function of the arc span-thickness ratio. Also in the present case, the accuracy of the proposed model decreases for low values of $L/2h$ and, in general, the error is slightly higher than that shown in Figure 11. However, for $L/2h > 50$, the error of the EET method is of the order of less than 2%.

5 A practical method to evaluate the EET parameters

In the examples of the previous Section, the shape function for the radial displacement could be easily determined analytically. However, the curvature of architectural glass panel may be quite complex [33, 11]), and for such cases it is not immediate to determine the

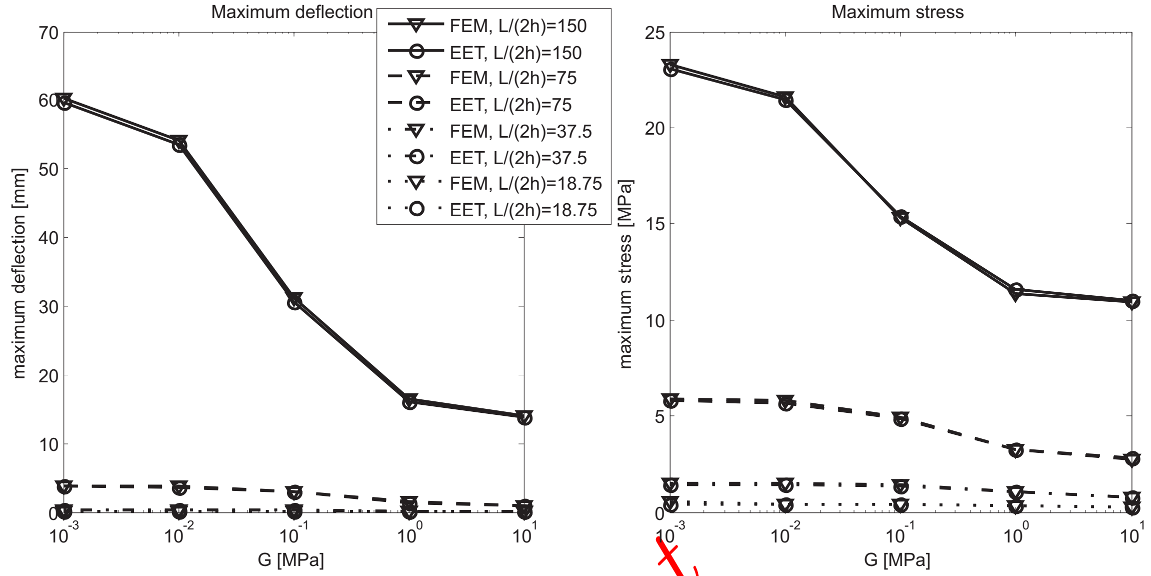

Figure 13: Circular arch with vertical constraints, under uniformly distributed radial load. Comparison of maximum deflection and maximum stress evaluated with the EET approach and the 3D FEM analysis, for different value of the span/thickness ratio.

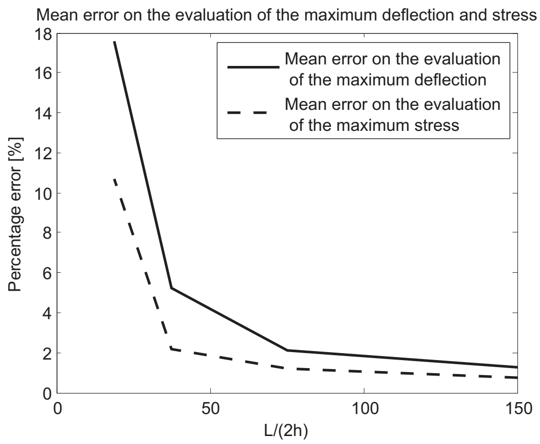

Figure 14: Circular arch with vertical constraints under uniformly distributed radial load. Mean percentage error in the evaluation of the maximum deflection and the maximum stress, as a function of the span/thickness ratio.

shape function analytically. In this Section it is shown how to calculate the EET parameters starting from the knowledge of the radial displacement in just a few points, obtained numerically or by an experimental campaign.

5.1 Evaluation of the parameter Υ

Referring to the non dimensional abscissa x defined as in (3.14) of Section (3.3), suppose that the radial displacement is known at points $x_k, k = 1, ..N$. These data can be interpolated with an analytic function, which can be used as a shape function to evaluate the coefficient Υ from (3.14).

For the case at hand, it is convenient to use a polynomial interpolation, which is infinitely regular. If the data points are N, there is exactly one polynomial of degree $N-1$ passing through all them. Suppose than to make the approximation

$$g(x) \simeq p_N(x) := \sum_{k=0}^{N-1} a_k\, x^k\,. \tag{5.1}$$

There are many ways to evaluate the coefficients a_k. A very practical one is to use Excel [31], by requiring the trendline from a plot or by using the regression function in the Data Analysis toolpack. Once such coefficient are known, the shear coupling coefficient Υ (3.14) may be calculated as

$$\Upsilon \simeq \Upsilon_N := \frac{\int_{-1}^{1} (p_{N,xx}(x))^2\, dx}{\int_{-1}^{1} (p_{N,x}(x))^2\, dx} = \frac{\sum_{k=2}^{N-1} \sum_{j=2}^{N-1} \frac{j(j-1)k(k-1)\ a_j a_k}{j+k-3}}{\sum_{k=1}^{N-1} \sum_{j=1}^{N-1} \frac{jk\ a_j a_k}{j+k-1}} \tag{5.2}$$

The minimum required number of data points is $N = 3$ because if the displacement is measured at two points only, the interpolating polynomial is linear and one would find $\Upsilon = 0$. This is because, roughly speaking, the shear coupling is associated with the the second derivative of the deformed shape. Explicit values of formula (5.2) for $N = 3, .., 6$ are summarized in Table 1.

Analysis of various practical examples indicates that, in order to obtain an accurate description it is usually sufficient to use a interpolating polynomial of degree 3 or 4, i.e., $N = 4$ or $N = 5$. When the deformed shape is symmetrical because geometry, load and boundary conditions are symmetrical, the accuracy of the interpolation may be increased by considering just half of the arch.

5.2 Examples and comparisons

In the following case-studies, a preliminary numerical analysis is made on a monolithic element of thickness $2h$, with area $2A$ and inertia comprised between the layered and mono-

N	Υ_N
3	$\dfrac{12a_2^2}{4a_2^2 + 3a_1^2}$
4	$\dfrac{60(3a_3^2 + a_2^2)}{27a_3^2 + 30a_1a_3 + 20a_2^2 + 15a_1^2}$
5	$\dfrac{84(36a_4^2 + 20a_2a_4 + 15a_3^2 + 5a_2^2)}{240a_4^2 + 336a_2a_4 + 189a_3^2 + 210a_1a_3 + 140a_2^2 + 105a_1^2}$
6	$\dfrac{36(500a_5^2 + 420a_3a_5 + 252a_4^2 + 140a_2a_4 + 105a_3^2 + 35a_2^2)}{875a_5^2 + 1350a_3a_5 + 720a_4^2 + 630a_1a_5 + 1008a_2a_4 + 567a_3^2 + 420a_2^2 + 315a_1^2}$

Table 1: Formulae for the evaluation of the coefficient Υ_N of (5.2), for specific values of N.

lithic limits, i.e. $I_L < \frac{b(2h)^3}{12} < I_M$, to determine the radial displacement at N points. Such values are used to estimate the coefficient Υ_N through (5.2) for different values of N, representing different degrees of approximation. Hence, the shear coupling coefficient η and the deflection- and stress-effective thicknesses can be calculated according to (3.14), (3.15), (3.16), respectively. Different-in-type geometries, boundary and loading condition, are considered. The results from the EET approach are compared with those calculate using the Wölfel-Bennison [7] formula (3.17), as well as with 3D numerical analysis performed with Abaqus [1].

5.2.1 Application to Example A. Accuracy of the approximate method

For the sake of comparison, the values of the coefficient Υ obtained *via* the approximation (5.2) are compared to those found in Section 4 with the correct shape function, analytically calculated. Figure 15a shows the data points and polynomial interpolations, performed with Excel, for the case of circular arch with radial constraints (Example A). The accuracy of the approximate method is evident in Figure 15b, which shows the values of Υ_N for $N = 3, .., 6$, evaluated by considering half of the arch due to symmetry, as well as the value calculated analytically in Section 4.1. It is evident from the graph that the approximate expression (5.2) gives excellent results for $N \geq 5$. For $N = 5$ the error is of order of 0.1%.

5.2.2 Example C. S-shaped curved beam under uniform pressure

The S-shaped curved beam of width $b = 1000$ mm, represented in Figure 16a, is formed by two circular arches of span 3000 mm and rise 250 mm, under a uniformly distributed pressure of 0.75 kN/m^2. The laminated package is the same of the previous examples. The boundary conditions are given by two vertical rollers at the extremities and one (unloaded) central constraint that serves only to avoid the rigid body displacement. The beam has been also analyzes numerically, using the mesh shown in Figure 16b, created by dividing the length in 120 elements and the width in 20 elements.

The shape function is estimated by interpolating the point data, as shown in Figure 17a. Figure 17b shows the coefficient Υ_N of (5.2) for various N. For $N = 6$ one obtains $\Upsilon_6 = 2.4692$. Because of the symmetry of the problem, a higher accuracy may be obtained

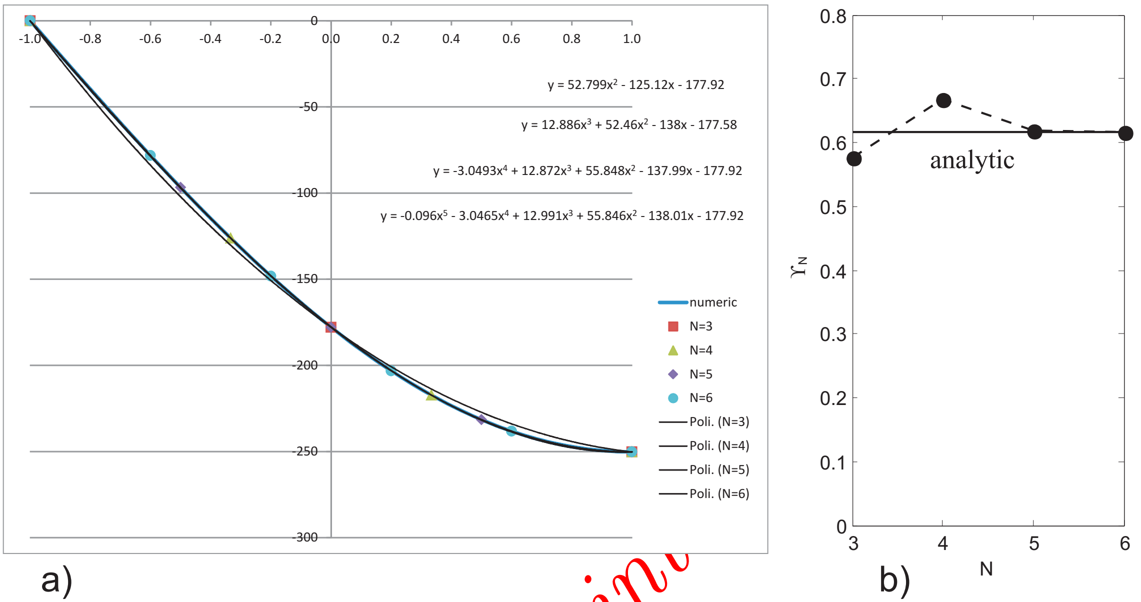

Figure 15: Circular arch under uniformly distributed radial load. a) Data points and interpolating polynomials; b) coefficient Υ_N as a function of N.

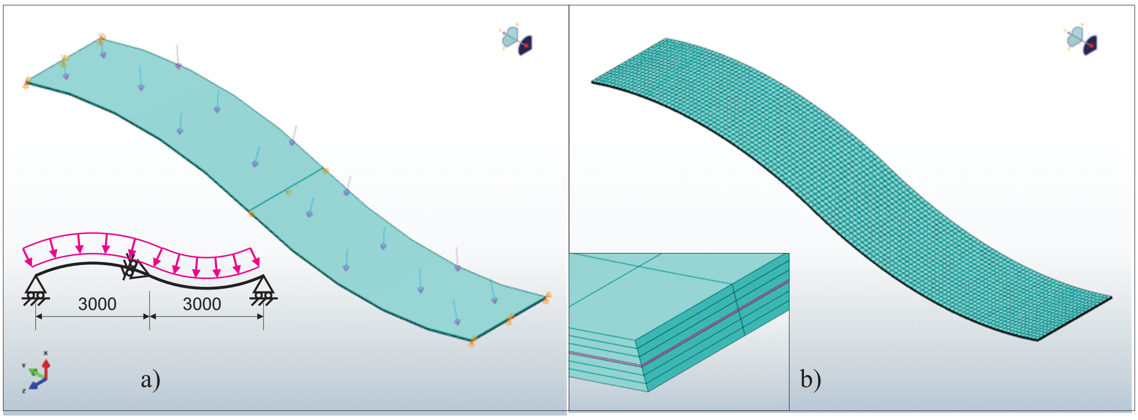

Figure 16: S-shaped curved beam under uniform pressure. a) geometry and b) mesh used in the FEM simulations.

by consider just half structure. Moreover, because of the low curvature, the radial and vertical components of the displacement field almost coincide: Figure 17b indicates that the values of Υ_N that can be obtained by considering the vertical displacement in practice coincide with those calculated from the radial displacement.

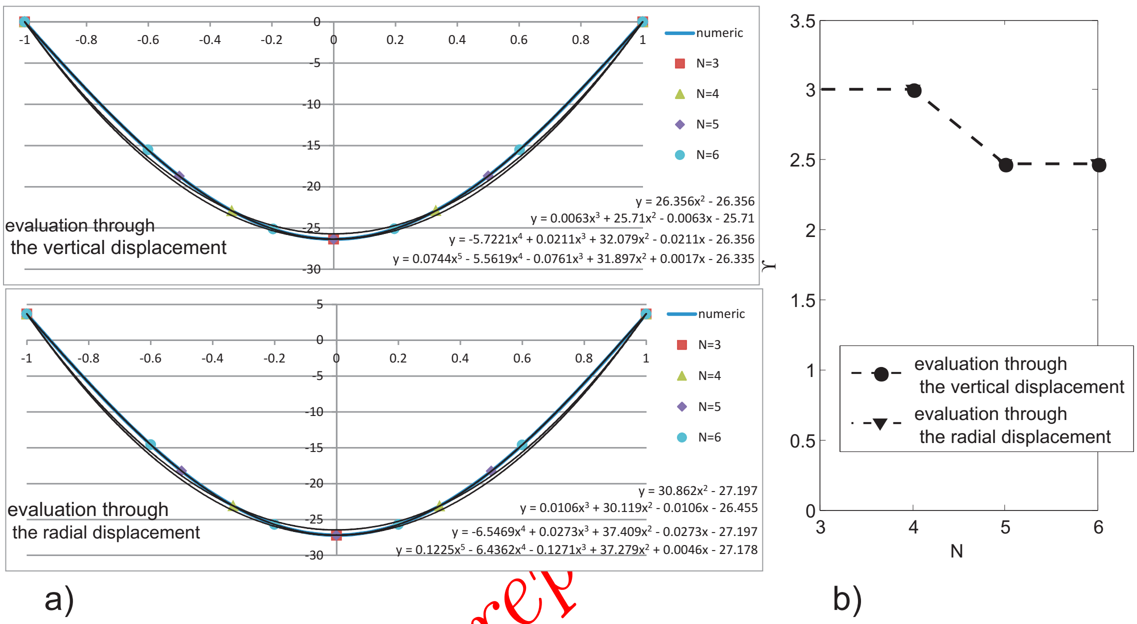

Figure 17: S-shaped curved beam under uniformly distributed pressure. a) Data points and interpolating polynomials; b) coefficient Υ_N as a function of the number N of data points.

The corresponding deflection and stress-effective thickness are plotted in Figure 18 as a function of G. The graph also shows the effective thicknesses predicted by the Wölfel-Bennison (WB) approach (3.17). No noteworthy differences are visible, because the curvature is moderate and the considered case is quite similar to a simply supported beam under uniformly distributed load, i.e., the case for which the WB approach is calibrated [17].

Figure 19 shows the comparison of the maximum stress and maximum deflection evaluated through the EET approach and the FEM analysis. Numerical results are in excellent agreement with the EET prediction, since the error is of the order of 0.5%.

5.2.3 Example D. Cantilever arch under concentrated load

Figure 20a shows a cantilever circular arch of width 1000 mm, length 1500 mm and rise 500 mm, subject to a concentrated load $F = 1000$ N at the free extremity. The laminated package is the same of the previous examples. The mesh for the FEM simulations, indicated in Figure 20b, has been created by dividing the length of the beam in 60 elements and the width in 30 elements.

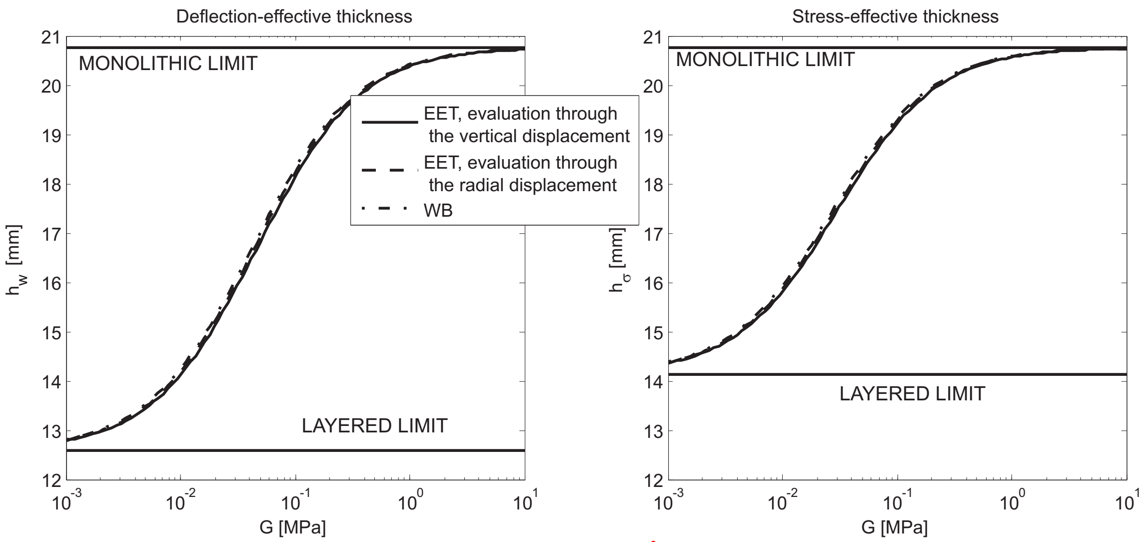

Figure 18: S-shaped curved beam under uniform pressure. Deflection- and stress-effective thickness evaluated through the EET model (considering either the radial of the vertical displacement) and the Wölfel-Bennison approach.

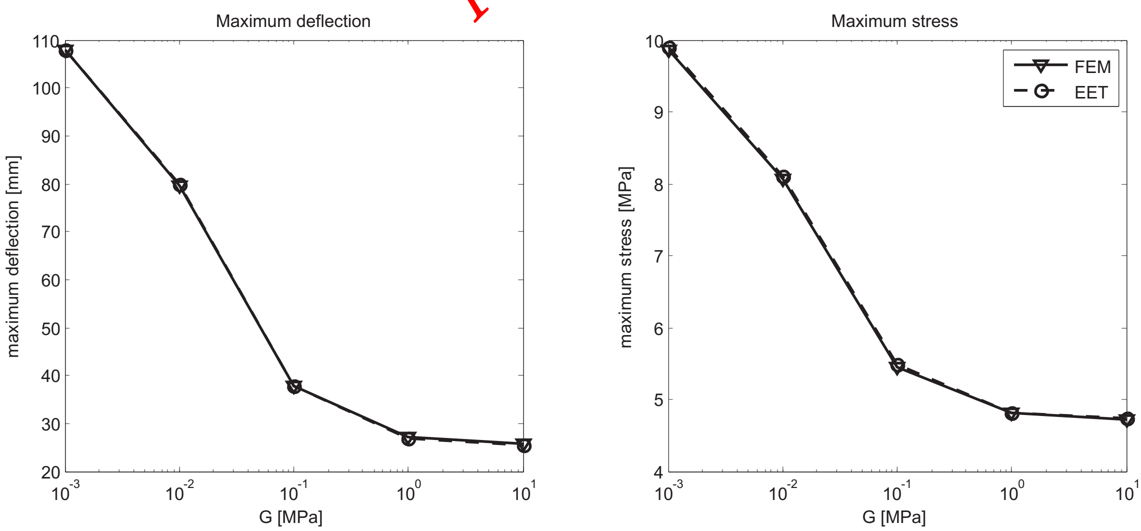

Figure 19: S-shaped curved beam under uniformed pressure. Maximum deflection and maximum stress evaluated with the EET model and the 3D FEM analysis.

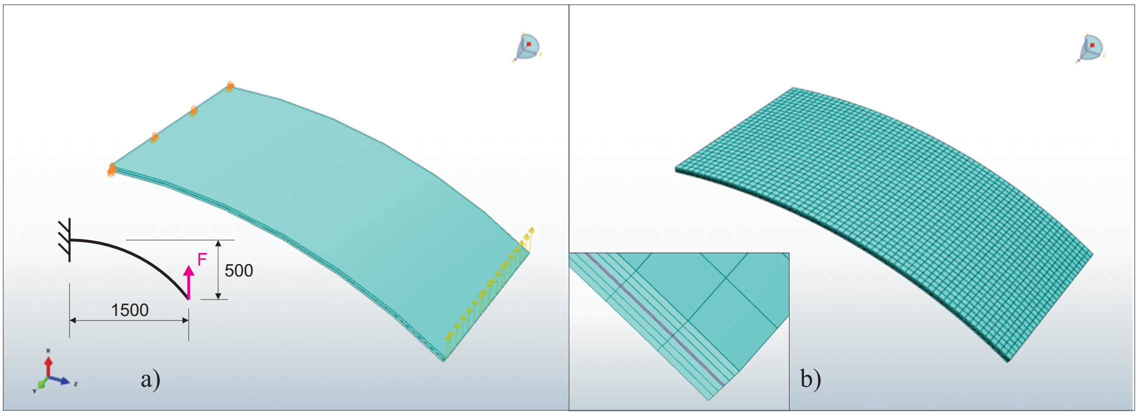

Figure 20: Cantilever circular arch under a concentrated load: a) geometry and b) mesh for the 3D FEM simulations.

The interpolating shape functions are shown in Figure 21a. Figure 21b shows the coefficient Υ_N for different values of N. Now a good approximation can be reached with a cubic interpolation function ($N = 4$), with $\Upsilon_4 = 0.6462$.

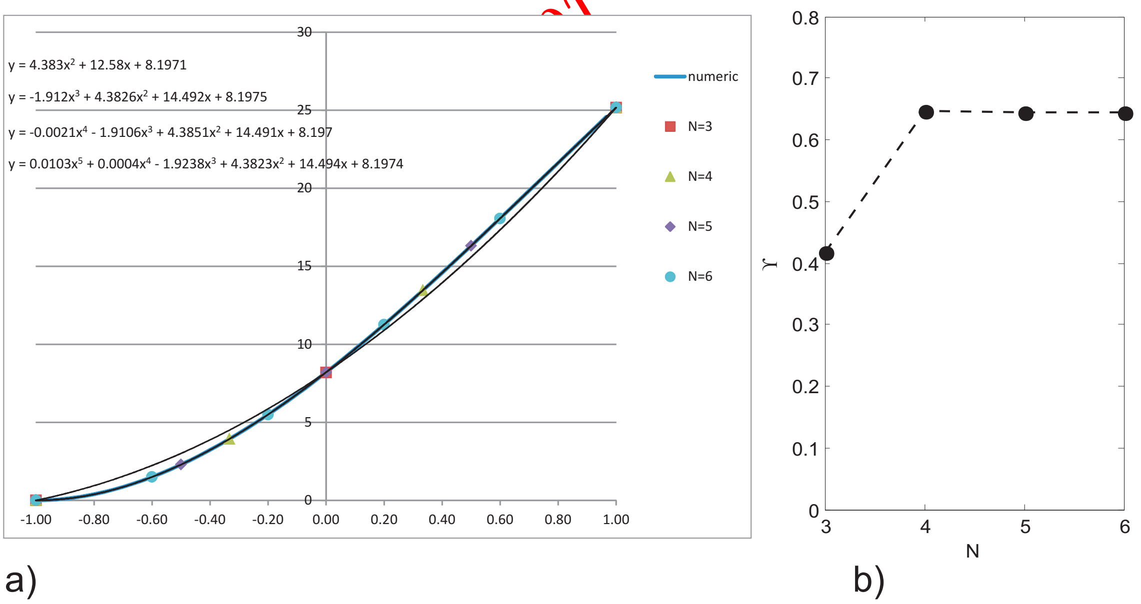

Figure 21: Cantilever arch under concentrated load. a) Data points and interpolating polynomials; b) coefficient Υ_N as a function of N.

Figure 22 shows the deflection- and stress-effective thickness. It is evident that now there is a noteworthy difference between the EET and the Wölfel-Bennison (WB) approaches. In fact, this case is substantially different from a simply supported beam under uniformly distributed load, which represents the benchmark configuration for the WB method.

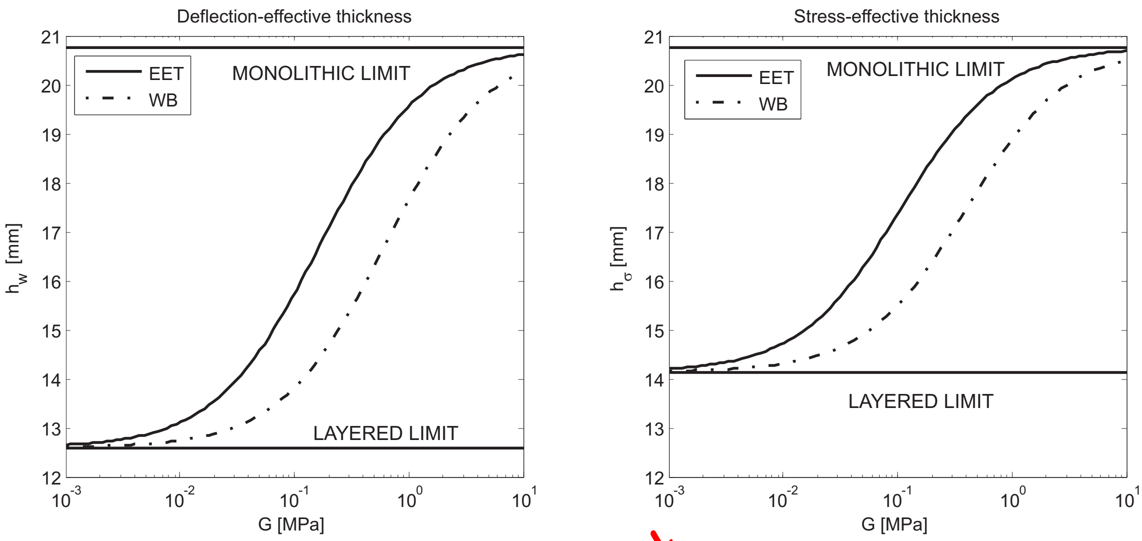

Figure 22: Cantilever arch under concentrated load. Deflection- and stress-effective thickness evaluated through the EET and the Wölfel-Bennison approaches.

In Figure 23 the maximum stress and maximum deflection are evaluated through the EET approach, the WB approach, and the 3D FEM analysis. The error of the EET approach with respect to the FEM experiments is of the order of 1% for deflection, and 2.5% for stress. The WB model is on the side of safety, but it is not accurate because the errors in the evaluation of the maximum deflection and stress are of the order of 20% and 6%, respectively.

5.2.4 Example E. Two-hinged arch

Consider the laminated glass two-hinged semicircular arch shown in Figure 24a, with radius of curvature of 1500 mm, under a concentrated load at the crown. The laminated package is the same as before. The FEM mesh is represented in Figure 24b , obtained by dividing the arc length in 120 elements, the arc width in 20 elements an the thickness of each glass plies in 3 elements.

Since the structure is symmetric, only half of it has been considered. Figure 25a shows the data points and the interpolating polynomials for the radial displacement. Figure 25b indicates the coefficient Υ_N as a function of N. In this case, a good approximation is reached with $N = 6$, for which Υ_6 5.9104.

In Figure 26, the deflection- and stress-effective thickness evaluated with the EET and the WB approaches are plotted as functions of G. In this case, the effective thicknesses from WB are consistently greater than those from the EET approach.

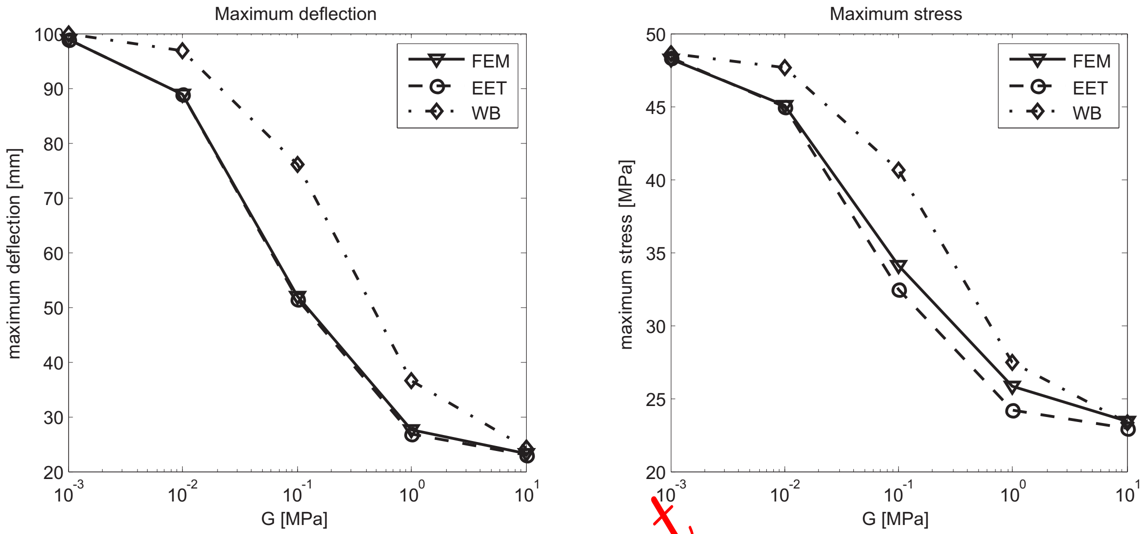

Figure 23: Cantilever arch under concentrated load. Comparison of maximum deflection and maximum stress evaluated with the EET model, the WB approach and FEM analysis.

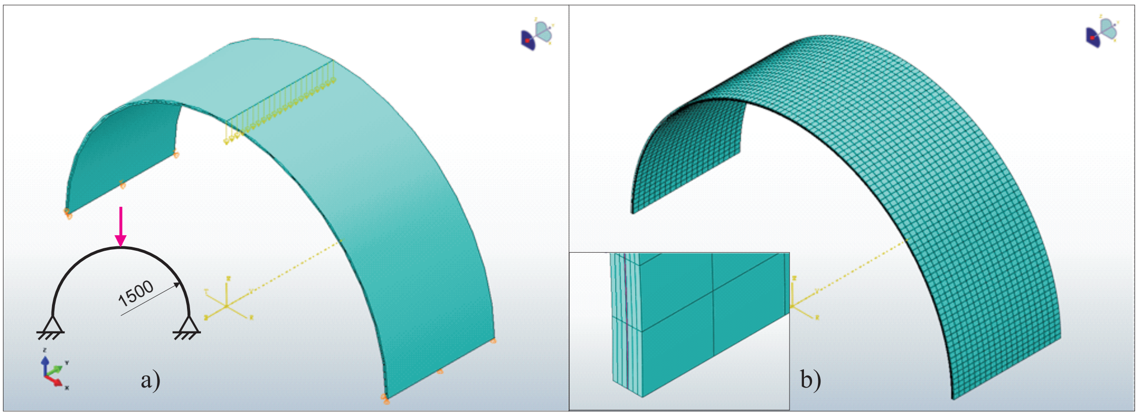

Figure 24: Two-hinged arch. a) geometry and b) mesh used in the 3D FEM simulations.

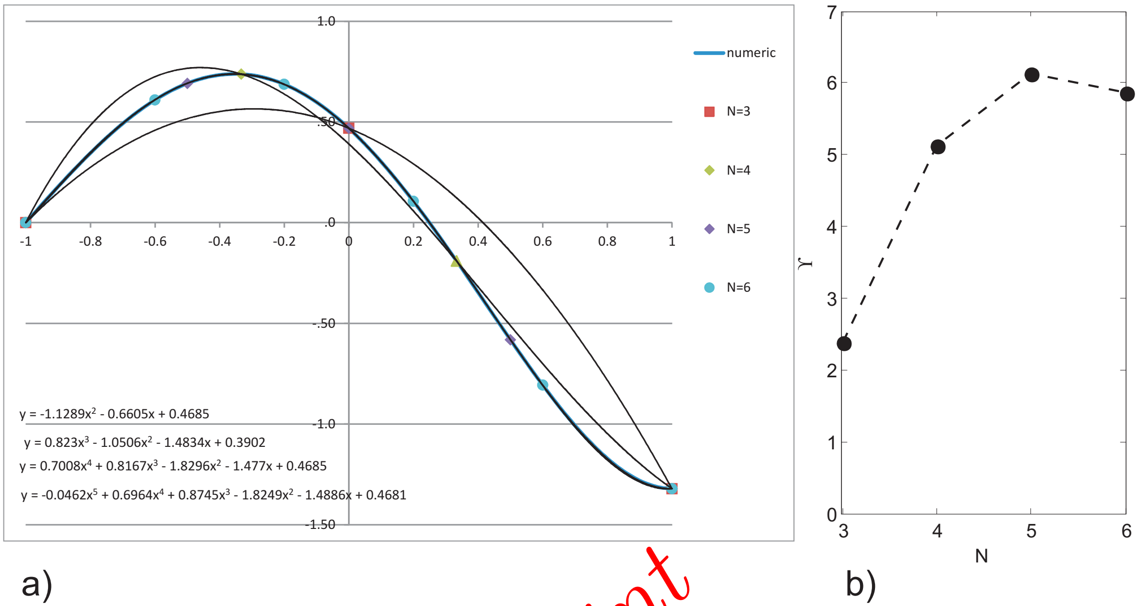

Figure 25: Two-hinged arch. a) Data points and interpolating polynomials; b) coefficient Υ_N as a function of N.

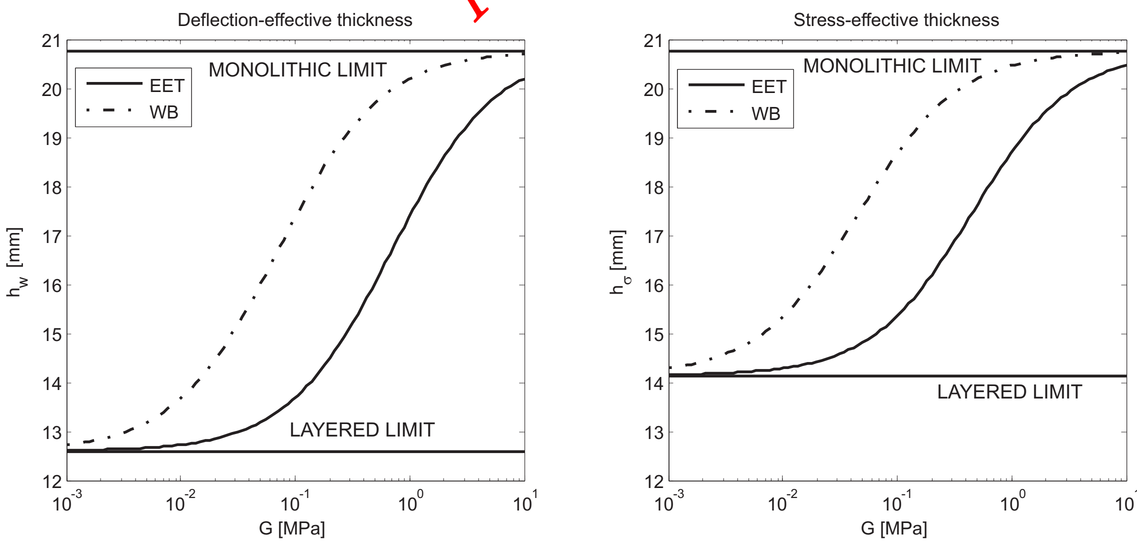

Figure 26: Two-hinged arch. Deflection- and stress-effective thickness evaluated through the EET model and the Wölfel-Bennison approach.

From Figure 27, which shows the comparison of maximum deflection and maximum stress evaluated with FEM analysis, EET and WB approaches, one can see that WB leads to a strong underestimation of both deflection and stress, with a mean error of the order of 20%, not on the side of safeness.

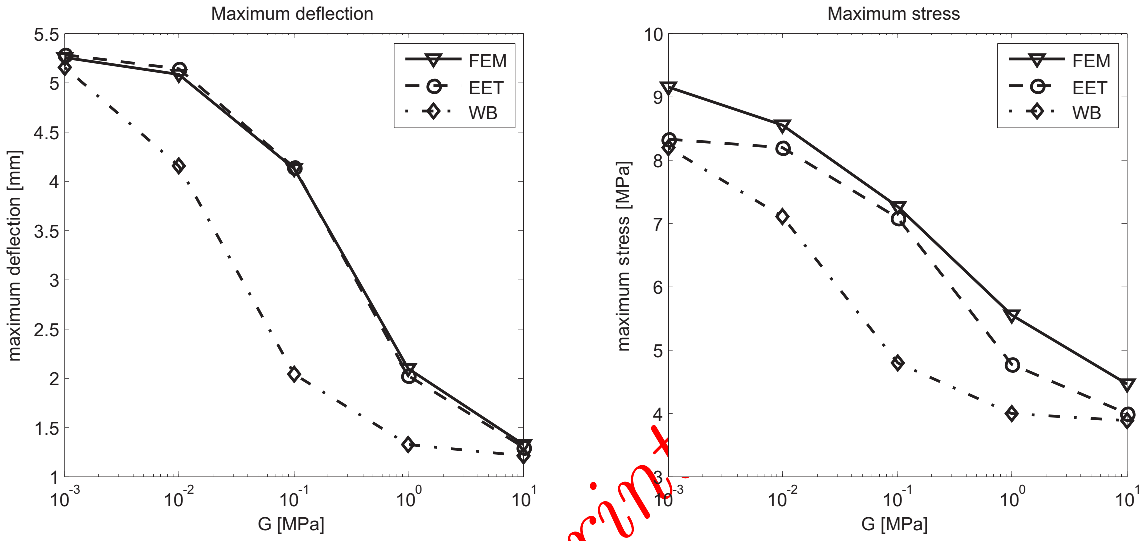

Figure 27: Two-hinged arch. Comparison of maximum deflection and maximum stress evaluated with EET and WB approaches, with 3D FEM simulations.

On the other hand, the agreement of the EET predictions with the numerical simulations is very good (mean error $\simeq 0.7\%$) for what concerns the maximal deflection. On the other hand, the EET method is less accurate for what the stress is concerned, especially close to monolithic and layered limit. This is due to the key assumption that in the EET approach the axial and flexural behavior do not influence each other. On the other hand, it is well known that in a hyperstatic arch, like the two-hinged static scheme, the axial strain influence the flexural response. In any case, the accuracy of the EET approach is consistently higher than the WB method.

6 Discussion and conclusions

The structural analysis of curved LG presents a strong additional difficulty with respect to flat LG because of the effects of the curvature, which complicates the kinematics associated with the shear coupling of the glass plies through the polymeric interlayer. A very effective and practical tool for the calculation of LG relies upon the determination of the deflection- and stress-effective thickness: this is a very practical definition, but different and sometimes conflicting formulations have been proposed in the literature. The most commonly used methods are the Wölfel-Bennison (WB) [7] and the Enhanced-Effective-Thickness (EET) [17] approaches, but all of them are conceived of for flat LG only. Here a theory is proposed that extends the EET approach to the case of LG panels with single curvature, treated by using curved-beam theory. A key hypothesis is to assume the uncoupling of the flexural and axial response of the laminated package, an assumption that is verified either if the curvature is very small, or if the structure is statically determined, so that the axial force in the beam is not influenced by its flexural response.

Simple formulas can thus be reached for the enhanced effective thickness of laminated glass. This depends upon a shape-function, representing the radial displacement of a monolithic curved beam with the same geometry, load and boundary condition of the laminated glass beam. Since only the ratio between its second-order and its first-order derivatives influence the relevant formulas, the shape function can be determined up to an irrelevant multiplying factor. Therefore, in most practical cases, to calculate the deformation, and hence the shape function, one can assume an arbitrary cross sectional inertia, provided it is comprised between the inertiae associated with the layered limit (free-sliding glass plies) or the monolithic limit (shear-stiff interlayer).

Paradigmatic case studies have been proposed to validate the proposed method. When the curvature is constant, the shape function can in general be determined analytically. When the structural scheme is more complex and/or the curvature is variable, it is not immediate to calculate the analytical expression of the shape function. Therefore, a practical approach has been proposed that consists in calculating the radial displacement in just a few points, and in interpolating the results with polynomials of appropriate order. The displacement data can be obtained by using any commercial numerical code, or could also be determined through experiments, in order to determine the effective thickness directly by testing. Explicit formulas are presented when the number of data points is up to 6, but in the considered examples just 4-5 points are sufficient to obtain reliable results. Comparisons with the results of accurate 3D numerical analysis with a FEM code confirm that the EET method for curved beams provides excellent results in the calculation of stress and deflection.

The unofficial practice of considering curved LG beams as straight beams in the calculation of the effective thickness is verified to be accurate in those cases when the curvature is very small, i.e., the beam is almost straight. For such cases one can use the standard EET method for flat LG [17], whereas the WB approach [7] is accurate when, in addition, the beam is simply supported and the load is uniformly distributed. When the curvature is moderate, but not negligible, the method here proposed presents noteworthy advantages in terms of accuracy. In general, results are excellent when the beam is statically determined or, more precisely, when the axial force in the beam can be determined independently of its flexural stiffness. When this is not the case, for example in a two-hinged hyperstatic arch where the thrust depends on both the axial and flexural response, the method is less accurate, but still acceptable. In the considered example, the error has been about 0.7% in the deflection and 6% in the stress evaluation. In cases of this kind, the use of the formulas for straight beams cannot be recommended.

Acknowledgements. Support of the European Community European Community under grant RFCS-RFSR-CT-2012-00026 "S+G" is gratefully acknowledged.

References

[1] ABAQUS. *Analysis users manual, version 6.10.* Simulia, 2010.

[2] L Ascione and F Fraternali. On the mechanical behaviour of laminated curved beams: a simple model which takes into account the warping effects. *Atti Accad. Naz. Lincei Cl. Sci. Fis. Mat. Natur. Rend. Lincei Matem. Appl.*, 1:223–233, 1990.

[3] L Ascione and F Fraternali. A penalty model for the analysis of curved composite beams. *Comput. Struct.*, 45:985–999, 1992.

[4] M Asik, E Dural, M Yetmez, and T Uzhan. A mathematical model for the behavior of laminated curved glass beams. *Compos. Part B-Eng.*, 58:593–604, 2014.

[5] M Asik and S Tezcan. A mathematical model for the behavior of laminated glass beams. *Comput. Struct.*, 83:1742–1753, 2005.

[6] R A Behr, J E Minor, and H S Norville. Structural behavior of architectural laminated glass. *J. Struct. Eng.-ASCE*, 119:202–222, 1993.

[7] S J Bennison and I Stelzer. Structural properties of laminated glass. In *Short Course, Glass Performance Days, Tampere (Finland)*, 2009.

[8] A Bhimaraddi, A J Carr, and P J Moss. Generalized finite element analysis of laminated curved beams with constant curvature. *Comput. Struct.*, 31:309–317, 1989.

[9] A. Blake. *Handbook of Mechanics, Materials, and Structures*, chapter Curved Members. Wiley Series in Mechanical Engineering Practice. Wiley, 1985.

[10] I Calderone, P S Davies, S J Bennison, H Xiaokun, and L Gang. Effective laminate thickness for the design of laminated glass. In *Glass Performance Days, Tampere (Finland)*, 2009.

[11] M Eigensatz, M Kilian, A Schiftner, N J Mitra, H Pottmann, and M Pauly. Paneling architectural freeform surfaces. *ACM Trans. Graph.*, 29:45:1–45:10, 2010.

[12] P Foraboschi. Behavior and failure strength of laminated glass beams. *J. Eng. Mech.-ASCE*, 133:1290–1301, 2007.

[13] P Foraboschi. Analytical solution of two-layer beam taking into account non-linear interlayer slip. *J Eng Mech - ASCE*, 135:1129–1146, 2009.

[14] Y Frostig. Bending of curved sandwich panels with a transversely flexible core - closed-form high-order theory. *J. Sandw. Struct. Mater.*, 1:4–41, 1999.

[15] L Galuppi, G Manara, and G Royer-Carfagni. Practical expressions for the design of laminated glass. *Compos. Part B - Eng*, 45:1677–1688, 2013.

[16] L Galuppi, G Manara, and G Royer-Carfagni. Erratum and addendum to practical expressions for the design of laminated glass (composites part b: Engineering (2013) 45 (1677-1688)). *Compos. Part B - Eng*, 56:599–601, 2014.

[17] L Galuppi and G Royer-Carfagni. Effective thickness of laminated glass beams. New expression via a variational approach. *Eng. Struct.*, 38:53–67, 2012.

[18] L Galuppi and G Royer-Carfagni. Laminated beams with viscoelastic interlayer. *Int J Sol Struct*, 49:2637–2645, 2012.

[19] L Galuppi and G Royer-Carfagni. The effective thickness of laminated glass plates. *J. Mech. Mater. Struct.*, 7:375–400, 2012.

[20] L Galuppi and G Royer-Carfagni. The design of laminated glass under time-dependent loading. *Int J Mech Sci*, 68:67–75, 2013.

[21] L Galuppi and G Royer-Carfagni. The effective thickness of laminated glass: Inconsistency of the formulation in a proposal of EN-standards. *Compos. Part B - Eng*, 55:109–118, 2013.

[22] L Galuppi and G Royer-Carfagni. Curved sandwich beams with shear compliant core. Part I: Basic equations. *Submitted for publication*, 2014.

[23] L Galuppi and G Royer-Carfagni. Curved sandwich beams with shear compliant core. Part II: Approximations and examples. *Submitted for publication*, 2014.

[24] L Galuppi and G Royer-Carfagni. Enhanced Effective Thickness of Multi-Layered Laminated Glass. *Compos. Part B - Eng*, 64:202–213, 2014.

[25] J A Hooper. On the bending of architectural laminated glass. *Int. J. Mech. Sci.*, 15:309–323, 1973.

[26] I V Ivanov. Analysis, modelling, and optimization of laminated glasses as plane beam. *Int. J. Sol. Struct.*, 43:6887–6907, 2006.

[27] National Research Council. *CNR-DT-210: Istruzioni per la progettazione, l'esecuzione e il controllo di costruzioni con elementi strutturali in vetro*. Project of Italian Stardard under Enquiry, 2012.

[28] N M Newmark, C P Siess, and I M Viest. Tests and analysis of composite beams with incomplete interaction. *Proc. Soc. Exp. Stress Anal.*, 9:75–92, 1951.

[29] H S Norville, K W King, and J L Swofford. Behavior and strength of laminated glass. *J. Eng. Mech.-ASCE*, 124:46–53, 1998.

[30] American Society Testing of Materials. *E1300-09a. Standard Practice for Determining Load Resistance of Glass in Buildings*. ASTM International, 2009.

[31] Microsoft Office.

[32] H Pottmann, Bo P, A Schiftner, H Schmiedhofer, N Baldassini, and J Wallner. Architectural freeform structures from single curved panels. *ACM Transactions on Graphics*, 27(3), 2008.

[33] Helmut Pottmann, Alexander Schiftner, Pengbo Bo, Niccolo Baldassini, Heinz Schmiedhofer, Wenping Wang, and Johannes Wallner. Freeform surfaces from single curved panels. *ACM transaction on graphics*, 27(3):76:1–76:10, 2008.

[34] H. Sagan. *Introduction to the Calculus of Variation*. Dover, New York, 1992.

[35] W.R. Spillers. *Introduction to Structures*. Woodhead Publishing Series in Civil and Structural Engineering. Elsevier Science, 2002.

[36] D.V. Wallerstein. *A Variational Approach to Structural Analysis*. A Wiley-Interscience publication. Wiley, 2002.

[37] E. Wölfel. Nachgiebiger verbund - eine näherungslösung und deren anwendungsmöglichkeiten. *Stahlbau*, 6:173–180, 1987.